**Author Contributions:**

**Conceptualization:** T. Delcroix, B. Malaizé
**Formal analysis:** T. Delcroix, S. L. L. Michel, D. Swingedouw, B. Malaizé, A.-L. Daniau, R. Abarca-del-Rio, T. Caley, A.-M. Sémah
**Methodology:** T. Delcroix, S. L. L. Michel, D. Swingedouw, B. Malaizé
**Software:** S. L. L. Michel, D. Swingedouw, T. Caley

# Clarifying the Role of ENSO on Easter Island Precipitation Changes: Potential Environmental Implications for the Last Millennium

**T. Delcroix[1]** , **S. L. L. Michel[2]** , **D. Swingedouw[3]** , **B. Malaizé[3]** , **A.-L. Daniau[3]** , **R. Abarca-del-Rio[4]** , **T. Caley[3]** , and **A.-M. Sémah[5]**

[1]LEGOS, UMR 5566 CNES/CNRS/IRD/Toulouse University, Toulouse, France, [2]IMAU, Department of Physics, Utrecht University, Utrecht, The Netherlands, [3]UMR 5805 EPOC, Bordeaux University, Bordeaux, France, [4]Department of Geophysics, Concepción University, Concepción, Chile, [5]UMR 7194, Muséum national d'Histoire naturelle, Paris, France

**Abstract** El Niño Southern Oscillation (ENSO) events yield precipitation deficits and ensuing droughts, often damaging regional forests, in many parts of the world. The relative roles of ENSO, other natural climate changes, and anthropogenic factors on the forest clearing of Easter Island over the last millennium are still debated. Here, we analyze Easter Island precipitation changes using in situ, satellite-derived and reanalysis products spanning the last 4–7 decades, and 46 monthly 156-year-long (1850–2014) simulations derived from 25 CMIP5 and 21 CMIP6 (Coupled Model Intercomparison Project phases 5 and 6) General Circulation Models. Our analysis shows that La Niña events, the cold phases of ENSO, cause precipitation deficits of −0.2 to −0.3 standard deviation (relative to long-term mean) in all analyzed data types. ENSO-like events are further examined over the last millennium (850–1981). A new multiproxy reconstruction of the NINO3.4 index based on proxy records from the Past Global Changes 2k database and Random Forest method is produced. Our reconstruction reveals unusual high recurrences of La Niña-like situations during the fifteenth to seventeenth centuries, which likely induced significant precipitation deficits on the island. These situations are compared to published vegetation reconstructions based on pollen analyses derived from sedimentary cores collected in three island sites. We conclude the environmental consequences of cumulative precipitation deficits over long-lasting La Niña-like situations reconstructed here over the fifteenth to seventeenth centuries were likely favoring drought and forest flammability. La Niña events should be better accounted for among the causes of forest clearing on Easter Island.

**Plain Language Summary** Easter Island is a small remote island located in the south-eastern Pacific Ocean. It is home of several scientific enigmas: the origin of early settlements, the construction of the giant moai statues, and causes of the forest clearing. Was the forest clearing abrupt, gradual, homogenous in time and space, human-induced (in line with the ecocide hypothesis), or related to natural climate variability? The question we address in this paper is related to the natural climate variability hypothesis, focusing on the El Niño Southern Oscillation (ENSO) phenomenon. We analyze ENSO effects on Easter Island precipitation from three instrumental (1950–2021) and 42-simulation data sets (1850–2014). Our analysis shows the cold phases of ENSO, also known as La Niña, cause significant precipitation deficits over the island in all analyzed data types. Then, we provide a new up-to-date reconstruction of ENSO over 850–1981. We found a large number of La Niña-like situations during the fifteenth-seventeenth centuries. These situations are compared to vegetation reconstructions derived from sedimentary cores collected in three island sites. We conclude that the environmental consequences of cumulative precipitation deficits during long-lasting La Niña-like situations could be an additional cause of the forest clearing of Easter Island.

## 1. Introduction

The Pacific Ocean covers more than a third of the world's ocean surface area, extending over about 45% of the Earth's circumference along the equator from 80°W to 120°E. The tropical band includes more than 20,000 high and low islands, often classified into three main groups as Melanesia, Micronesia, and Polynesia. The decline and extinction of palm forests from the late Pleistocene have been demonstrated for most of these islands using palaeoecological records (Preble & Dowe, 2008). The likely causes for the extinction include climate change, abrupt climatic events, droughts, invasive fauna and flora species, geological activity, and human colonization.

**Supervision:** T. Delcroix
**Validation:** S. L. L. Michel, D. Swingedouw
**Writing – original draft:** T. Delcroix, S. L. L. Michel, D. Swingedouw, B. Malaizé, A.-L. Daniau, R. Abarca-del-Rio, T. Caley, A.-M. Sémah
**Writing – review & editing:** T. Delcroix, S. L. L. Michel, D. Swingedouw, B. Malaizé, A.-L. Daniau, R. Abarca-del-Rio, T. Caley, A.-M. Sémah

Quantifying the respective role and impact of these causes and their interactions is a very complex issue. Easter Island, the easternmost island of Polynesia, is undoubtedly an emblematic example of such an issue. It was sometimes considered a microcosm of our planet regarding the hypothetical use by locals of natural resources in a non-sustainable manner (e.g., Diamond, 2005).

Easter Island, also known as Rapa Nui in the Polynesian language, is located at 27°07′S and 109°21′W (see Figure 1). Covering an area of 164 km², the island has a triangular shape with sides of the order of 15–25 km. There are three crater lakes, sources of consumable freshwater, one in each corner: the Rano Aroi in the North, the Rano Raraku in the East, and the Rano Kau in the Southwest (Figure 2). The island remained uninhabited for centuries, except for temporary visits, until it was colonized from eastern Polynesia during the still-discussed timeframe covering the eighth to eleventh century (e.g., Hunt & Lipo, 2006). Research to date indicates that the island was fully forested in the late Pleistocene (Flenley & King, 1984). It has been proposed that gradual forest clearing occurred between 800 and 1200 and the decades to centuries before 1700, a few years before the recorded first European contact in 1722 (see Rull, 2020).

Information about the forest decline of Easter Island comes mainly from analyses of sediment cores collected in the three main crater lakes of Rano Kao, Rano Raraku, and Rano Aroi. Fossil pollen, charcoal traces, and sometimes rare earth elements from these cores have been examined in various papers to reconstruct past vegetation and fire occurrences. A summary of related results is given in Table 1 for the three crater lakes, and a synthetic diagram for the Rano Aroi is in Figure 3. Rano Aroi is the highest elevated crater lake and likely the last area of the island to be deforested and settled (Flenley et al., 1991). Table 1 clearly highlights the complexity of the information provided by the existing literature, and an apparent lack of consensus regarding the timing of the forest decline over the island. This partly reveals that forest decline was not homogeneous in space and time over the Island (Rull, 2020). For the Rano Aroi, Figure 3 shows that palm woodland with shrubs was present until about 1300, followed by a palm forest development until about 1500. The period about 1550–1700 is marked by intense droughts corresponding to substantial redox conditions (high Fe/Al ratio) (Roman et al., 2021), the disappearance of the palm forest and a grassland development (Rull et al., 2015). However, the exact timing of these environmental changes remains uncertain, given the estimated error of 100–350 years of the age models from Roman et al. (2021) and Rull et al. (2015).

Despite many works and studies, the timing and causes accounting for the disappearance of the palm-dominated forest are still amply debated and challenged in the literature. Forest demise was first viewed as caused mainly by human activities, in particular, to free space for agriculture development, to get rolls of wood for transportation of the giant moai statues, to construct dwellings and canoes, and firewood for cooking (Flenley & King, 1984; Bahn & Flenley, 1992, updated in 2019). This interpretation has led to the hypothesis of an irrational over-exploitation of the forest leading to a "collapse" (or "ecocide") of the ancient Rapa Nui civilization (see Diamond, 2005, and the references therein). The Rapa Nui undoubtedly cut down some trees, but the collapse hypothesis is far from being collectively accepted (e.g., Boersema, 2015; Cauwe, 2018; DiNapoli et al., 2021; Rull, 2020; Stevenson et al., 2015). For instance, another view is that forest decline was partly caused by palm seed consumption by rats introduced by Polynesians, preventing their regeneration (Hunt, 2007; Hunt & Lipo, 2011). The influence of climate change has also been partially explored. The main examined candidates were drier climate, long-lasting precipitation shortage, and droughts associated with either the Medieval Warm Period (MWP, ≈950–1250), the Little Ice Age (LIA, ≈1200–1850) and/or the El Niño Southern Oscillation (ENSO) variability (M. E. Mann et al., 2009; Orliac & Orliac, 1998; Rull, 2020).

In most parts of the world, the mean and variability of precipitation shape vegetation greening, persistence, and fire risk (Linscheid et al., 2020; Van der Werf et al., 2008). What do we know about precipitation in the tropical Pacific? Schematically, in steady state, due to the Coriolis force, north-easterly trade winds blow in the northern hemisphere, and south-easterly trade winds blow in the southern hemisphere. These trade winds converge onto the Inter-Tropical Convergence Zone (ITCZ), stretching roughly along 10°N, and onto the South Pacific Convergence Zone (SPCZ), extending roughly from Papua New Guinea to French Polynesia. The trade winds system results in accumulation of a large volume of warm (>28.5°C) waters in the upper 50–70 m to the western Pacific warm pool. Due to Ekman divergence, the dominant westward components of the trade winds result in the occurrence of colder (20–22°C) surface waters in the East in the so-called equatorial upwelling. In this steady state, high precipitation (>0.25 m/month) is found in the ITCZ, SPCZ, and the western Pacific warm pool, which are all regions of intense atmospheric convections (Figure 1). Regions of relatively low precipitation (<0.04 m/month)
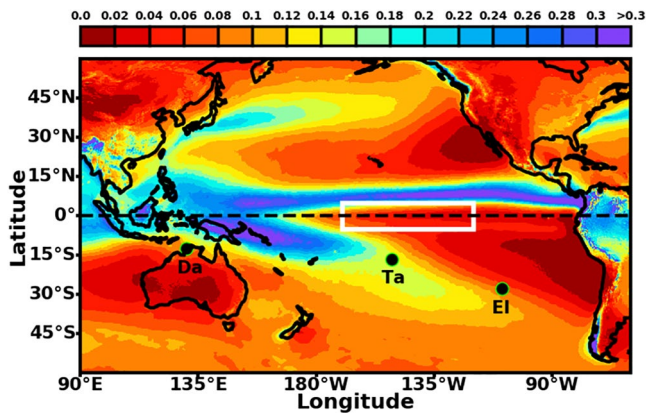
**Figure 1.** Spatial distribution of 1950–2021 averaged ERA5 precipitation. Unit is m/month. Black letters denote Darwin (Da), Tahiti (Ta), and Eastern Island (EI) positions. The white rectangle delimits the NINO3.4 region.



**Figure 2.** Mean annual precipitation over Easter Island, with color codes in mm/year. Also shown as thin black lines are the topographic isolines with 100 m contour levels. The blue square denotes the Mataveri meteorological station position. Black letters K, A, and R, show the positions of the Rano Kao, Rano Raraku, and Rano Aroi crater lakes, respectively. Adapted from Stevenson et al. (2015).

are observed in the north-eastern and south-eastern tropical Pacific, the latter region including Easter Island.

The variability of precipitation in the tropical Pacific occurs at different time scales. At seasonal time scales, the largest precipitation changes occurred around the mean position of the ITCZ and SPCZ. This results from the seasonal swing of the related heavy rainfall bands, which are both shifted 5°–10° poleward (equatorward) during their summer (winter) hemisphere (Hsu & Wallace, 1976). At the ENSO interannual time scale, during "conventional" El Niño events, we observe below-average precipitation in some kind of boomerang-shaped area stretching from Papua New Guinea toward north and south higher latitudes, and above-average precipitation around the equatorial band with extreme anomalies near the date line (Philander, 1989; see also Figure S1 in Supporting Information S1). These El Niño changes mainly result from the equatorward shifts of the ITCZ-SPCZ, and eastward shift of the western Pacific warm pool (Picaut et al., 1996; Tchilibou et al., 2015). The reverse anomalies happened during La Niña events. Noteworthy, the precipitation signature of ENSO can differ markedly at both regional and global scales from one event to another. This is especially the case for the so-called Eastern (EP) and Central Pacific (CP) El Niño events for which the maximum warm sea surface temperature (SST) anomalies appeared in the eastern or central equatorial Pacific, respectively (Ashok et al., 2007; Kug et al., 2009). Basin-scale studies indicate precipitation changes are much smaller during CP El Niño events. They are also of opposite signs to those of EP El Niño events in the central and eastern equatorial regions, with negligible EP-CP differences nearby Easter Island (Kao & Yu, 2009; Singh et al., 2011).

At the decadal time scale, the main documented precipitation changes are linked to the Pacific Decadal Oscillation (PDO; Newmann et al., 2016) or Interdecadal Pacific Oscillation (IPO; Salinger et al., 2001). These modes have been shown to be related to an asymmetric distribution of El Niño and La Niña events (Power et al., 2021; Rodgers et al., 2004). Then, the positive (negative) phases of the PDO or IPO mostly show up as El Niño-like (La Niña-like) situations, with associated spatial anomalies in precipitation that are similar to the ones related to El Niño or La Niña events. Whether decadal variations are consequences of, or trigger, El Niño and La Niña asymmetry, and what is the role of external processes are still open questions (Power et al., 2021; T. Sun & Okumura, 2020), but at least they are intimately related to the frequency of occurrences of those events (Newman et al., 2016). On a longer time, historical documents, model results, and proxy records (Grothe et al., 2019; M. E. Mann et al., 2009; Ortlieb, 2000) suggest ENSO and decadal variabilities were well present during the last millennium. There are, however, still debated interpretations regarding ENSO phases. For instance, M. E. Mann et al. (2009) indicate that the MWP was more La Niña-like than the LIA, contrary to the results of Yan et al. (2011).

As noted above, the forest decline of Easter Island has been viewed as either human-induced, related to precipitation changes linked to natural climate variability, or caused by a synergy of impacts. The question we want to address in this paper is related to the natural climate variability hypothesis, with an emphasis on the often-neglected potential influences of ENSO. The few published analyses of El Niño and La Niña effects on Easter Island are summarized in Table 2. They are based on different data sources and methods and reach different conclusions. Also, most published results have looked at the time correlation between ENSO phases and Easter Island precipitation anomalies, although they have rarely focused on the relative amplitude and duration of precipitation anomalies. Can ENSO play an important role in the local precipitation variability and in particular on drought episodes?

To bring pieces of answer to the above question, our paper is organized as follows. Data sets and methodology are described in Section 2. The relationships between Easter Island precipitation and ENSO variability, including
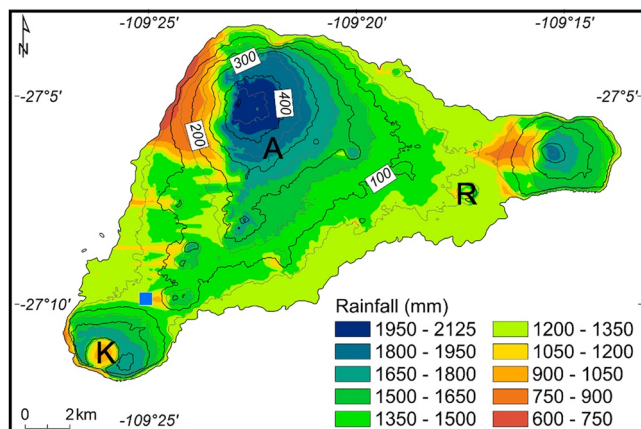
**Table 1**
*Summary of Key Results Discussing Forest Decline Timing and Likely Causes During the Last Millennium Over Easter Island*

| | References | Main data sets | Main results |
|---|---|---|---|
| 1 | De Lesseps (1861) | Visual observations (9 April 1786) | Hypothesize that the island was once forested |
| 2 | Heyerdahl and Ferdon (1961) | Sample cores from Rano Kao and Raraku | Easter Island had been forested. No dating is possible |
| 3–4 | Flenley and King (1984). Dransfield et al. (1984) | Pollen records from Rano Aroi, Kao, and Raraku | Palm forests established since late Pleistocene. Forest decline during the last millennium, likely human-induced |
| 5 | Orliac and Orliac (1998) | Samples of carbonized materials | Replacement of wood with grass in traditional ovens by about 1650. Likely role of abrupt climate changes. ENSO drought |
| 6–7 | Bahn and Flenley (1992, 2019) | Review past research, including their own | Massive forest decline caused by human factors. Collapse of megalith construction, the moai, around 1650 |
| 8 | Diamond (2005) | Theoretical work about the evolution of civilizations | Deforestation prior to European contact due to over-exploitation of natural resources. Ecocide |
| 9 | Hunt (2007) | Rat bones and palm endocarps | Forest affected by a synergy of impacts. Likely role of introduced rats on major native plants |
| 10 | D. Mann et al. (2008) | Pollen. Charcoal fragments. Rano Raraku | Palms decrease, and charcoal concentration increases by 1200 |
| 11 | Canellas-Bolta et al. (2013) | Multi-proxies. Rano Raraku | Forest decline pulses by 1200, 1450. Drought phases during 500–1200 and 1570–1720 |
| 12 | Rull et al. (2015) | Multi-proxies. Rano Aroi | Forest decline started during the sixteenth century; coinciding with fire increases. Dry climate by 600–1100 and 1520–1700 |
| 13 | Seco et al. (2019) | Pollen, Rano Kao | Forest decline pulses by 1070, 1410, 1600. Forest totally removed by 1600; coincides with fire increase |
| 14–15 | Rull (2020, 2021) | Thorough review. Rano Aroi, Kao, and Raraku | Forest decline is gradual, and not simultaneous over the island |
| 16 | Roman et al. (2021) | Trace and rare Earth Elements. Rano Aroi | Wet conditions 0–1400; Intense droughts 1520–1710; Intense precipitation 1790–1900 |

*Note*. Years in the right column were estimated from radiocarbon dating and specific age-depth models for sedimentary cores.

EP and CP El Niño and La Niña types, are then analyzed in Section 3, using three contemporary data products spanning the last 4–7 decades, and 46 1.5-century-long simulations (1850–2005) derived from 25 CMIP5 and 21 CMIP6 (Coupled Model Intercomparison Project, Phase 5 and 6) historical simulations of General Circulation Models (GCMs). Estimation of 850–1981 ENSO-like occurrences at times of forest changes is then analyzed in Section 4, based on a new reconstruction of the ENSO-related SST-NINO3.4 index produced for this study, that is based on state-of-the-art optimal statistical method using multiple proxy records. In the last section, we summarize our key results, compare the estimated past ENSO-like occurrences to vegetation reconstructions (as in Figure 3) estimated from published pollen analyses of sedimentary cores collected on the island, and discuss limitations and perspectives.

## 2. Data Sets and Methodology

### 2.1. Contemporary Climate Data Sets

Current precipitation data sets are usually based on satellite-derived observations, reanalysis products, in situ observations, and combinations of these data types. In this paper, we test three different precipitation products (out of at least 30 currently available global precipitation data sets, see Q. Sun et al., 2018) covering the last 4–7 decades: (a) the 1979–2020 CMAP (CPC Merged Analysis of Precipitation) data from the 2.5° latitude × 2.5° longitude monthly resolved field (Xie & Arkin, 1997), (b) the 1950–2021 monthly averaged 0.25° latitude × 0.25° longitude ERA5 reanalysis product from Hersbach et al. (2020), and (c) the 1939–2021 monthly averaged data computed from daily in situ observations collected at the Mataveri station (details about the Mataveri data are given in Supporting Information). The nearest CMAP and ERA5 grid points of 27°S-109°W are chosen to represent Easter Island precipitation.

Since ENSO spectral properties mostly range in the 3-to-7-year band (Tourre et al., 2001), the times series of 30–70 years of precipitation discussed above is relatively short to properly analyze the ENSO signal. We
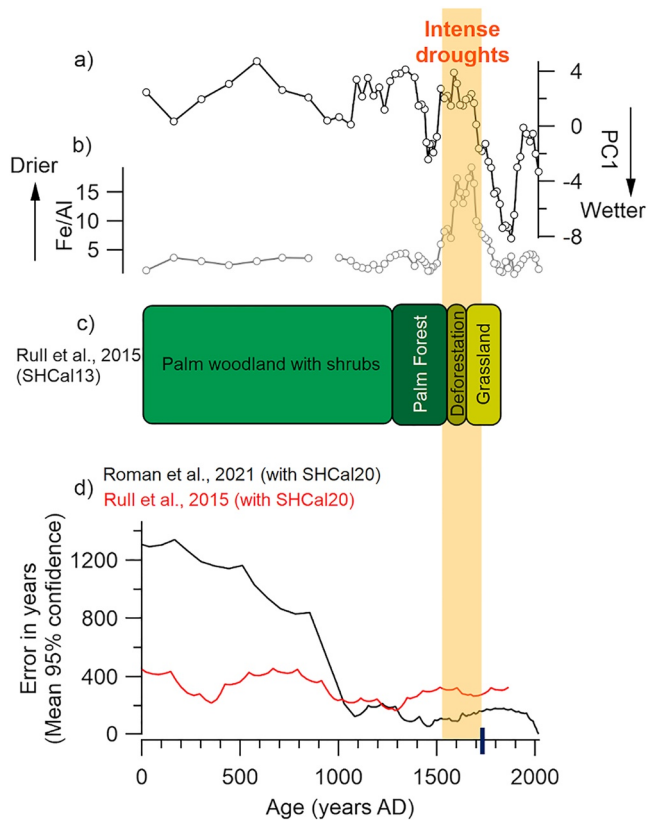
**Figure 3.** Summary of key Rano Aroi geochemical/vegetational climate reconstructions over the last 2000 years (a) First principal component (PC1) of major and trace elements in the sediment interpreted as terrestrial input (Roman et al., 2021). (b) Fe/Al ratio as a proxy for redox conditions indicating intense droughts occurring during the middle Little Ice Age between 1520 and 1710 (Roman et al., 2021). (c) Main vegetation changes (Rull et al., 2015). (d) Errors in years (mean 95% confidence) (this study) for the age model of Roman et al. (2021) and Rull et al. (2015) based on ¹⁴C ages converted to calibrated ages using the SHCal20 calibration curve (Hogg et al., 2020) with the depth-age model using Bayesian accumulation histories for deposits (BACON) software for modeling (Blaauw & Christen, 2011) in R (R Core Team, 2019). The heavy black tick on the time axis shows the date of first European contact on 6 April 1722.

thus additionally rely on a much more extended period, covering about 1.5 centuries. For this purpose, we extracted monthly resolved SST and precipitation fields derived from 25 CMIP5 GCMs (Taylor et al., 2012) covering the years 1850–2005 and 21 CMIP6 GCMs (Eyring et al., 2016) covering the years 1850–2014. These models are those whose outputs were loaded in the Institut Pierre Simon Laplace (IPSL) Earth System Grid Federation (ESGF) node and available at the time of writing. Information about these GCMs, including their atmospheric grid resolution, is given in the Table S1 in Supporting Information S1. All model ocean grids were interpolated onto a common 1°latitude × 1° longitude grid resolution. The nearest GCM grid points of 27°S–109°W are chosen to represent Easter Island. The relative ability of GCMs to properly simulate the main basin-scale ENSO features is discussed in Bellenger et al. (2014) for the CMIP5 and Planton et al. (2021) for the CMIP6 simulations.

We identified long-term trends in the precipitation fields in some of the GCM simulations. For consistency, the time series of all contemporary climate data sets were thus linearly detrended over their respective time period in order to focus on interannual variability related to ENSO changes and not long-term climate change signals. The statistical significance for correlation coefficients discussed below is performed by accounting for autocorrelation correction in the computation of the degrees of freedom of the Student $t$-test, as in Michel et al. (2020) and based on statistical tests from Bretherton et al. (1999). It avoids detecting spurious significant correlations, which artificially increase when time series are low-pass filtered.

### 2.2. Determining ENSO, ENSO Types, and IPO Phases

Numerous standard indices can reveal the timing and amplitude of ENSO phases (e.g., Hanley et al., 2003). Here, we use the SST-NINO3.4 index that denotes the spatially averaged SST in box 170°W–120°W and 5°S–5°N (see Figure 1). Using SST-NINO3.4 is comparable to the frequently used atmospheric southern oscillation index (SOI), as these two indices vary consistently, though in opposite signs. El Niño (La Niña) is characterized by a 3-month running mean of SST-NINO3.4 that is above (below) the threshold of +0.5 (−0.5) standard deviation for five consecutive months. The tropical Pacific is otherwise in a neutral situation. The threshold of ±0.5 standard deviation is adopted to homogenize ENSO phases definition over the different record lengths to be analyzed. Using a threshold of ±0.5°C of SST-NINO3.4 anomalies (relative to a mean monthly year computed over a fixed record length)

as in the National Oceanic and Atmospheric Administration (NOAA) operational definitions for El Niño/La Niña gives similar results. The SST-NINO3.4 is computed from the HadISST product (Rayner et al., 2003) for the 1870–2021 period and each GCM's gridded monthly SST field for the period 1850–2014. Possible biases in using a fixed NINO3.4 region in GCMs to infer ENSO changes are discussed in Section 4. The Multivariate ENSO Index (MEI, Wolter & Timlin, 2011) is also discussed below when considering the quasi-linear relationship between the amplitude and the duration of ENSO phases.

Different methods and indices have been used to contrast the EP and CP ENSO types. The SST-based indices include the Trans-Niño Index (TNI; Trenberth & Stepaniak, 2001), the El Niño Modoki Index (EMI; Ashok et al., 2007), and the CP Index (Kao & Yu, 2009). These indices agree with each other (see Singh et al., 2011; their Figure 1). Here, we use the EMI, which is the difference between the area-averaged SST anomalies (SSTA) over the region A (10°S–10°N, 165°E−140°W) and the average of the SSTA in the region B (15°S–5°N, 110°W−70°W) and C (10°S–20°N, 125°E−145°E). The EMI thus captures the tripolar nature of some ENSO events. As a result, when the EMI is positive, the ENSO event is classified as a CP event, and when it is negative as an EP event, regardless of whether it is an El Niño or La Niña event.

**Table 2**
*Summary of Key Results Discussing the Role of ENSO on Easter Island Environmental Changes*

| | References | Period (yr) | Data | Main results |
|---|---|---|---|---|
| 1 | McCall (1993) | | Speculations | Suggest possible El Niño effects. No mention of La Niña |
| 2–3 | Orliac and Orliac (1998), Orliac (2000) | | Discussion | ENSO and related drought could play a role in forest decline in the mid-seventeenth |
| 4 | MacIntyre (2001) | 1985–1993 | NCEP NCAR maps | No El Niño effects on SST and P near Easter Island |
| 5 | Trenberth and Caron (2000) | 1979–1998 | CMAP, SOI (Annual means) | Co-occurrence of La Niña (El Niño) events and negative (positive) P anomalies near Easter Island |
| 6 | Mucciarone and Dunbar (2003) | 1945–1995 | Coral core | El Niño signature on reconstructed SST offshore Easter Island. |
| 7 | Genz and Hunt (2003) | 1950–2000 | Mataveri, MEI (Annual means) | $R = 0.3$ between P and the MEI. $R = 0.89$ for the seven strongest La Niña |
| 8 | Yan et al. (2011) | 1979–2010 | NCEP, SOI, P reconstruction | Same as (4). Tropical Pacific is more La Niña-like during the LIA |
| 9 | Junk and Claussen (2011) | 800–1750 | MPI GCM | $R = 0.28$ between P over Easter Island and NINO3.4. |
| 10 | Delcroix et al. (2018) | 1982–2015 | CMAP, NINO3.4 (Interannual anomalies) | $R = 0.6$ between P over Easter Island and NINO3.4. Key role of La Niña on P deficit |
| 11 | Lima et al. (2020) | 1961–2015 | Mataveri, SOI (Annual means) | $R = -0.34$ between P and the SOI |
| 12 | Steiger et al. (2022) | 1955–2017 | Mataveri (daily values) | No relationships between the number of large rain events and ENSO |

*Note*. P stands for precipitation. R in the right column is the correlation coefficient.

The IPO is measured by the Tripole Index (TPI) of Henley et al. (2015), which is the difference between the SSTA in the tropical central Pacific (10°S–10°N, 170°E–90°W) and the average of the extratropical SSTA in the southwest (50°S–15°S, 150°E–160°W) and northwest (10°S–10°N, 170°E–90°W) Pacific.

The 25-month Hanning filtered and standardized SST-NINO3.4, EMI, and IPO time series are shown in Figure 4. That filter removes intraseasonal and seasonal variabilities and therefore facilitates detection of ENSO and IPO fingerprints. The filter passes almost no signal at periods of 1 year and less but passes about 90% of the signal at 4 years. Delcroix (1998, his Figure 1) illustrates its effects on times series dominated by intraseasonal, seasonal and interannual (ENSO) variability. Looking at the SST-NINO3.4 in Figure 4, we identify very strong El Niño events in 1982–1983, 1997–1998, and 2015–2016 (the highest on record), and strong La Niña events in 1988–1989, 1998–1999 (extended in 1999–2000) and 2010–2011. The high correlation ($R = 0.91$) between the SST-NINO3.4 and IPO confirms the dominance of El Niño situations during the positive phases of the IPO, and La Niña situations during the negative phases.
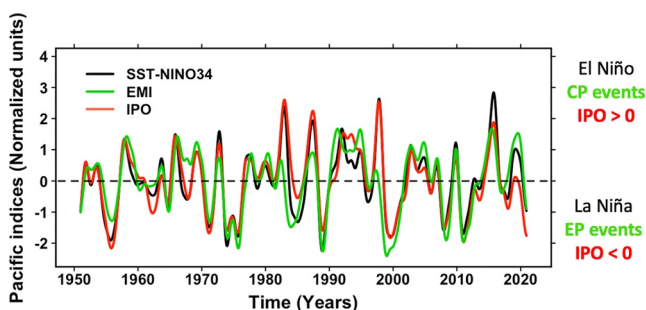


**Figure 4.** Standardized sea surface temperature-NINO3.4, El Niño Modoki Index, and Interdecadal Pacific Oscillation time series over the period 1951–2021. All indices have been smoothed with a 25-month Hanning filter for clarity.

### 2.3. Reconstruction of Pre-Industrial ENSO Variations

Multiple paleo-proxy reconstructions of ENSO exist in the literature (e.g., Dätwyler et al., 2020; Emile-Geay et al., 2013a, 2013b, 2020; Li et al., 2013; M. E. Mann et al., 2009; McGregor et al., 2013; Yan et al., 2011). They differ

from each other because they use different ENSO timing, ENSO definitions, instrumental data sets to build predictands, proxy records, and statistical methods to make reconstructions. Here, we decide to update these reconstructions using the latest version of the PAGES 2k database (PAGES 2k Consortium, 2017), therefore including almost all proxy records available to reconstruct the ENSO index. Also, we propose using advanced statistical methods that are accounting for a non-linear relationship between predictor and predictand within the reconstruction phase: the random forest approach. For this purpose, the Climate Index Reconstruction software (Michel et al., 2020) was used to derive several reconstructed SST-NINO3.4 time series covering the last millennium. Numerous reconstructions were obtained by combining different methods and sets of proxy records according to their temporal coverage (cf. Michel et al., 2020; Michel, Swingedouw, Ortega, et al., 2022). We utilized a large initial set of 554 annually resolved proxy records, essentially composed of proxy records from the PAGES 2k database. The reconstruction models were computed by shuffling:

- Four different regression methods: principal component regression, partial least squares, elastic-net and random forest (Michel et al., 2020; Michel, Swingedouw, Ortega, et al., 2022).
- A total of 31 possible time windows on which to build the model (i.e., the learning period): from 1870 to 1970 to 1870–2000, with an 1-year increment for the upper bound. Since regression methods cannot adequately handle missing data, the objective of this parameterization is to empirically solve the dilemma of whether to use a large number of historical data that will be covered by a smaller number of proxy records (i.e., longer learning period), or the opposite (i.e., shorter learning period).

For each statistical model, only the proxy records that correlate with the SST-NINO3.4 time series significantly at the 95% confidence level over the learning period are used for the reconstruction. The 84 derived reconstructions were evaluated using the Coefficient of Efficiency (CE) metric (Nash & Sutcliffe, 1970) for 30 training/testing splits. The regression method and timeframe for building the statistical model leading to the higher score for the reconstruction reaching back to 850 is then kept as the optimal model. The model is then applied for a number of interlocking reconstruction timeframes (i.e., nested reconstruction), the first starting from 850 and the last starting in 1869 (i.e., the first year with SST observations), with a 1-year increment between each. This approach thus leads to the use of an increasing amount of proxy records as more of them become available as the target timeframe of reconstruction shortens (Michel, Swingedouw, Ortega, et al., 2022).

The final nested reconstruction (Figure 5) was obtained using the random forest method up to 1981. It is based on 54 proxy records collected within and around the Pacific basin, consistent with the target NINO3.4 SST index (see Figures 5c and 5d). Regarding CE scores, their consistently significant average over time indicates that the statistical model we built provides a reliable reconstruction (Figure 5b; Nash & Sutcliffe, 1970). Interestingly, the CE scores barely change over time, even when the Coral data are incorporated from about 1600, indicating the longest proxy records used for the reconstruction have quite strong reconstruction skills.

## 3. Contemporary Precipitation and ENSO Variability

In this section, we (re-) document Easter Island precipitation's mean and seasonal variability as a background and analyze the "present-day" relationships between precipitation and ENSO. The analysis is performed on precipitation and SST data sets from 1950 to 2021 (Section 3.1) and 1850–2014 (Section 3.2) using usual statistics. To have a large-scale view, we further examine basin-wide ENSO-related precipitation changes for CMAP, ERA5, the CMIP5 NorESM1-M GCM outputs from the Norwegian Climate Center (Bentsen et al., 2013), and the CMIP6 CESM2 Community Earth System Model from the National Center for Atmospheric Research (Danabasoglu et al., 2020). These two models were chosen for illustrative purposes but also due to their overall good representation of ENSO properties (see Bellenger et al., 2014; Planton et al., 2021).

### 3.1. What Do the 1950–2021 Observations Tell Us?

Mean annual precipitation in the tropical Pacific from ERA5 is shown in Figure 1. There are relatively low precipitation regions in the north-eastern and south-eastern tropical Pacific. The latter region borders Easter Island, located far from the ITCZ influence and on the north-eastern extension of the SPCZ. The mean precipitation over Eastern Island is $0.059 \pm 0.048$, $0.069 \pm 0.051$, and $0.093 \pm 0.069$ m/month for the 1979–2020 CMAP, 1950–2021 ERA5, and 1939–2021 Mataveri data sets, respectively (the second number is the standard deviation of the monthly time series). Similar values were obtained for the common 1979–2020 period ($0.071 \pm 0.055$ for
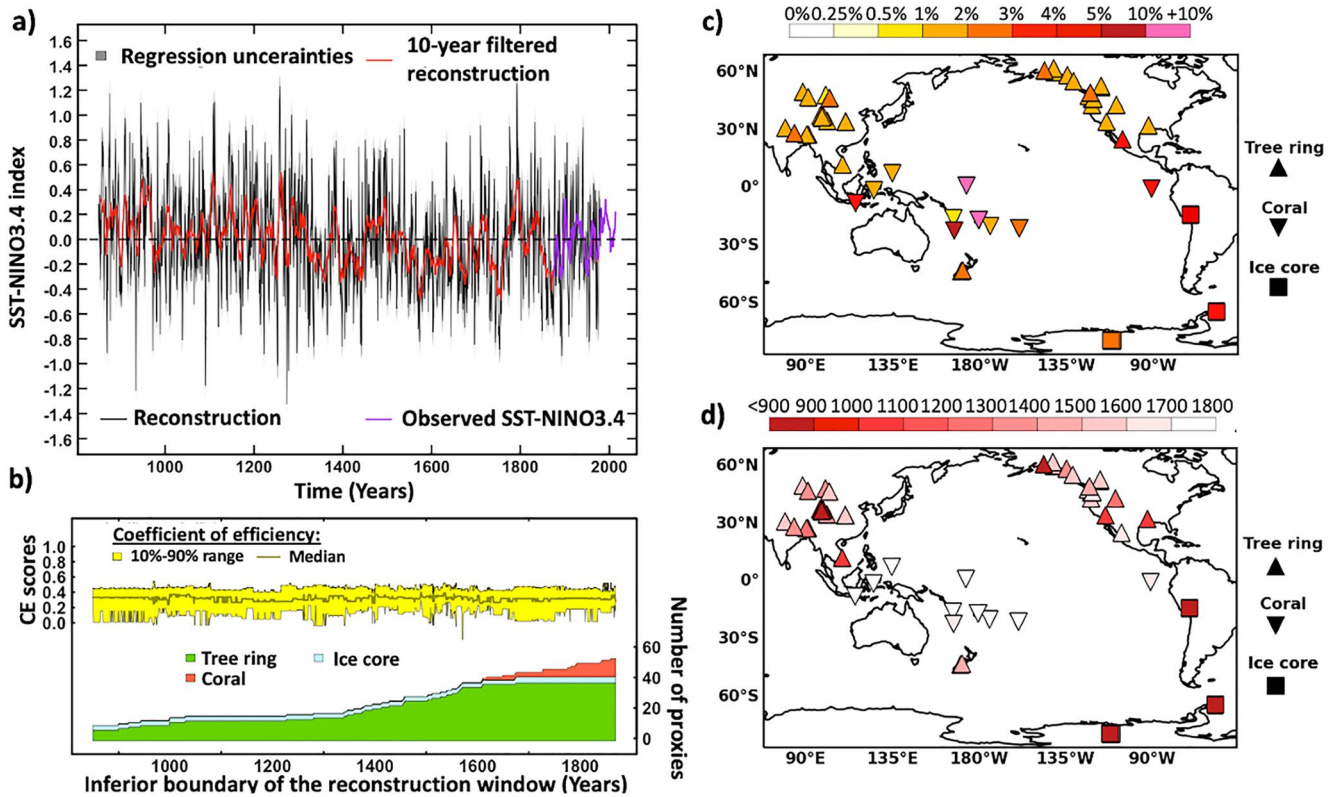
**Figure 5.** (a) Black line: reconstructed sea surface temperature (SST)-NINO3.4 index. Gray areas: regression error bars defined as a two-standard error spread. The derived red line is the 10-year Hanning filtered SST-NINO3.4 reconstruction, and the purple line is the instrumental 10-year filtered SST-NINO3.4. (b) yellow area: 10%–90% spread of coefficient of efficiency (CE) scores for each timeframe of the nested reconstruction as obtained for 30 training/testing sample splits. The yellow-gray line denotes the median CE score over the 30 training/testing splits. The bottom areas give the amount per type of proxies used over time. (c) Spatial distribution map of the proxy records used for the reconstruction. The above color bar denotes their weights given as random forest importance relative to their temporal coverage. (d) Spatial distribution map of the proxy records used for the SST-NINO3.4 reconstruction. The above color bar denotes their temporal coverage in years.

ERA5, $0.096 \pm 0.074$ for Mataveri). As expected, the two gridded products (CMAP and ERA5), which are more representative of spatial averages over their respective grid mesh, underestimate the value obtained from the Mataveri point measurements. There is no permanent station-based precipitation network that can monitor spatial variations over Easter Island. Occasional precipitation time series indicate large differences in mean precipitation depending on the topography, with changes of the order of $+0.02$ m/month per 100 m elevations (Figure 2). Thus, there is a potential bias in interpreting Mataveri as representative of the entire island (as also discussed below).
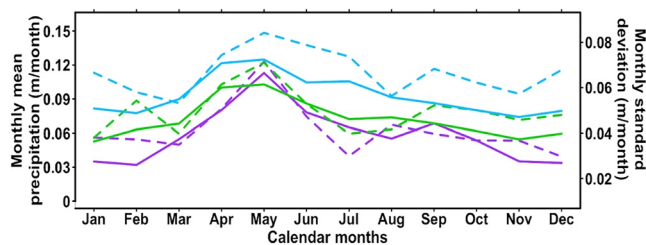
The monthly mean years and corresponding standard deviations of precipitation computed from the CMAP, ERA5, and Mataveri data sets are shown in Figure 6. Maximum precipitation values happen in April-May-June and minimum values in December-January-February, whatever the data sets. Interestingly, the monthly mean standard deviations are about 50% of the monthly means, indicating substantial changes from 1 year to the other, suggesting possible ENSO effects.

The general relationship between Easter Island precipitation and SST-NINO3.4 is illustrated in Figure 7 for the raw (i.e., unfiltered) monthly CMAP data set. The scatter plot shows a slight tendency for lower precipitation values to occur during colder-than-average SST-NINO3.4 (hence, partly during La Niña events) and higher precipitation values during warmer-than-average SST-NINO3.4 (hence, partly during El Niño events). This tendency also shows up as a quasi-linear relationship between precipitation and SST-NINO3.4 when precipitation values are averaged in



**Figure 6.** Monthly mean year (full lines) and corresponding monthly standard deviation (dashed lines) of precipitation over Easter Island, as computed from the CPC Merged Analysis of Precipitation (purple), ERA5 (green), and Mataveri (light blue) data sets. Note the different vertical scales. Units are m/month.
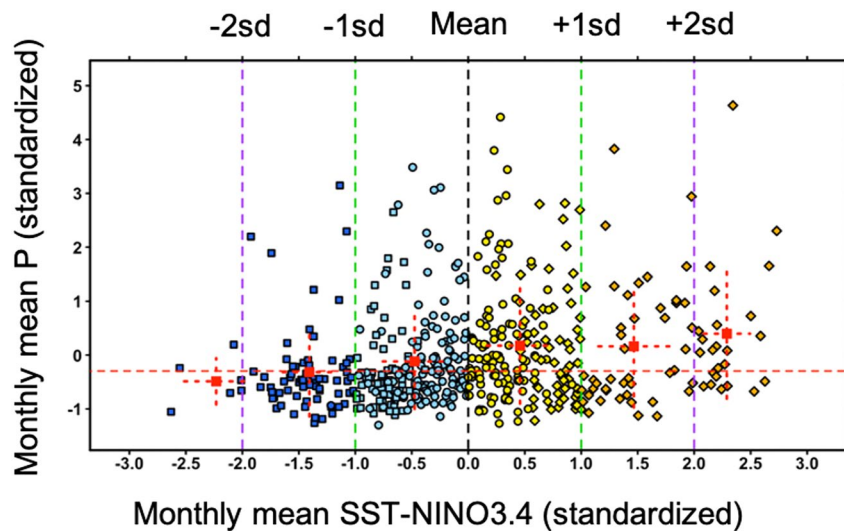
**Figure 7.** Scatter plot of the monthly CPC Merged Analysis of Precipitation standardized precipitation as a function of the standardized sea surface temperature (SST)-NINO3.4 index. Circles, diamonds, and squares, respectively, indicate neutral, El Niño, and La Niña situations, according to the definition in Section 2.2. The six red squares and related dashed red lines denote the means and related standard deviations in precipitation and SST-NINO3.4 computed over each of the six sub-scatter plot intervals delimited by vertical dashed lines denoting standard deviation (sd) multiples. The dashed horizontal red lines indicate the mean precipitation values during La Niña situations.

SST-NINO3.4 standard deviation intervals. However, the scatter plot indicates a relatively large spread of precipitation values, especially within −1 and +2 standard deviations of the mean SST-NINO3.4 (also visible with the ERA5 and Mataveri data sets, not shown here). This underlines, for instance, that some El Niño events (say when SST_NINO3.4 is above 0.5 standard deviation) do not necessarily correspond to above-average precipitation. The relationships between SST-NINO3.4 and precipitation are thus more complex than a simple linear one. Three metrics, D1, D2, and D3, are then computed to specifically clarify La Niña effects on Easter Island precipitation shortage:

- $D1$: The difference of standardized averaged precipitation during La Niña states against those during neutral ENSO states;
- $D2$: The difference of standardized averaged precipitation during La Niña states against those during El Niño states;
- $D3$: The difference of standardized averaged precipitation during La Niña states against those during either El Niño or neutral ENSO states.

These three metrics are computed from precipitation and SST-NINO3.4 anomalies (relative to their respective monthly climatology) to subtract the mean seasonal cycle influences because the timing of the monthly climatology in SST-NINO3.4 is roughly in phase with the timing of precipitation over Easter Island. The anomalies are standardized to estimate precipitation changes in terms of standard deviation. Remarkably, all $D1$, $D2$, and $D3$ values (Table 3) consistently indicate negative precipitation anomalies during La Niña states compared to all other situations, with precipitation deficits reaching values of the order of −0.2 to −0.4 standard deviation. Based on the monthly 1870–2021 SST data, we found an average duration of La Niña events of 13.5 ± 7.4 months, with a tendency for one event to be followed by another event (see Hu et al., 2014), hence extending the related precipitation deficits over time.

To complement the scatter plot and appreciate variations in time of the relationships found, we compare the detrended and 25-month Hanning filtered SST-NINO3.4 to the CMAP, ERA5, and Mataveri Easter Island precipitation (Figure 8) over their 1979–2020 common period. Correlation coefficients between the SST-NINO3.4 and the CMAP, ERA5, and Mataveri time series are $R = 0.55$, 0.39, and 0.17, respectively (Table 3). The weakest correlation is obtained for Mataveri which might be linked with the inhomogeneity (smoothed with the gridded CMAP and ERA5 products) of the ENSO signature over Easter Island, due to its complex topography. This interpretation is in agreement with Nicet and Delcroix (2000)'s findings (e.g., their Figure 5), which showed that

**Table 3**
*Main Statistics Related to the Easter Island Precipitation Changes*

|      | CMAP  | ERA5          | Mataveri      | CMIP5          | CMIP6          |
| ---- | ----- | ------------- | ------------- | -------------- | -------------- |
| $R$  | 0.55  | 0.39 (0.27)   | 0.17 (0.12)   | $0.33 \pm 0.17$  | $0.47 \pm 0.18$  |
| $D1$ | −0.41 | −0.39 (−0.25) | −0.19 (−0.28) | $-0.33 \pm 0.16$ | $-0.28 \pm 0.14$ |
| $D2$ | −0.52 | −0.37 (−0.33) | −0.15 (−0.22) | $-0.42 \pm 0.23$ | $-0.44 \pm 0.22$ |
| $D3$ | −0.44 | −0.38 (−0.29) | −0.17 (−0.26) | $-0.15 \pm 0.10$ | $-0.20 \pm 0.10$ |

*Note. R* is the correlation coefficient between the 25-month Hanning filtered and detrended SST-NINO3.4 index and Easter Island precipitation times series. *D*1, *D*2, and *D*3 are the standardized averaged precipitation changes during La Niña states against those during neutral ENSO states, El Niño states, and out of La Niña states, respectively. Numbers in the CMAP, ERA5, and Mataveri columns are computed from the 1979–2020, 1950–2021, and 1939–2021 monthly time series, respectively. Numbers in the CMIP5 and CMIP6 columns are computed from the monthly 1850–2014 time series; the second numbers are the inter-model standard deviations. Correlation coefficients and differences of standardized precipitations are all significant at the 90% confidence level, based on Student *t*-test. Values in brackets for ERA5 and Mataveri are statistics for the common period with CMAP.

ENSO-related precipitation changes differ markedly over the complex topography of the New Caledonia archipelago (≈22°S–166°E).

To evaluate the EP and CP ENSO differences on Easter Island precipitation, Figure 9 shows the 25-month Hanning filtered and detrended ERA5 precipitation over 1950–2021. Overplotted are the time distribution of EP and CP El Niño and La Niña events determined from the EMI values shown in Figure 4. As in Figure 8b, there is an overall tendency for positive precipitation anomalies during El Niño events and negative precipitation anomalies during La Niña events. Noteworthy, the 1950–2021 averaged precipitation anomalies are greater during EP than during CP La Niña. In contrast, they are statistically identical during CP and EP El Niño. Similar conclusions were obtained using the TNI, the CMAP, and Mataveri data sets (not shown here).
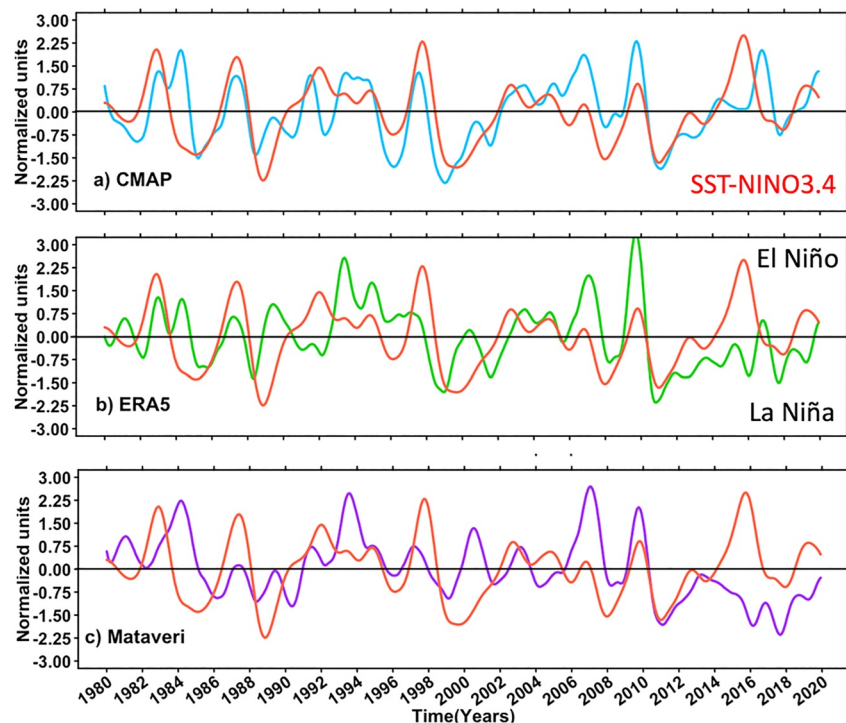


**Figure 8.** Time series of the 25-month Hanning filtered and detrended SST-NINO3.4 (red lines) and Easter Island precipitation computed from the CPC Merged Analysis of Precipitation (a, blue line), ERA5 (b, green line), and Mataveri (c, purple line) data sets. Tics on the *x*-axis denote the beginning of the years. All series have been standardized.
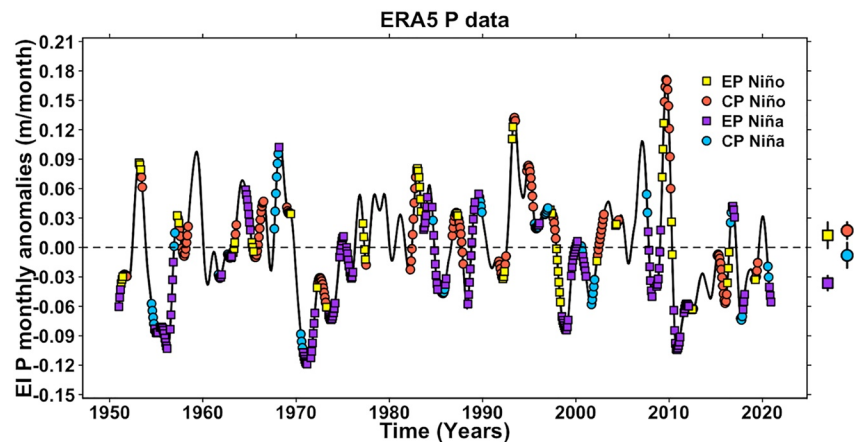
**Figure 9.** Time series of the 25-month Hanning filtered and detrended ERA5 precipitation anomaly over Easter Island (black line). Yellow squares on the black line denote EP El Niño; orange circles CP El Niño, purple squares EP La Niña, and blue circles CP La Niña. The 1950–2021 averaged EP and CP anomalies are shown on the right, with the whiskers representing the 95% level confidence intervals.

Correlation coefficient maps between SST-NINO3.4 and the precipitation fields of the CMAP and ERA5 data sets are shown in Supporting Information (Figures S1a and S1b in Supporting Information S1) for the tropical Pacific to have a large-scale view. They all indicate Easter Island falls within a Pacific-wide region extending from the NINO3.4 region to the east and the south-eastern Pacific, including Easter Island.

### 3.2. What Do the 1850–2014 GCM Simulations Tell Us?

Values of correlation coefficients ($R$) between the detrended and 25-month Hanning filtered Easter Island precipitation and SST-NINO3.4 simulated time series are shown in Figure 10 for the 25 CMIP5 and 21 CMIP6 GCMs. Also shown are the $D1$, $D2$, and $D3$ metrics defined above, with mean values given in Table 3. The multi-model mean correlation coefficients are $R = 0.33 \pm 0.17$ for the CMIP5 and $R = 0.47 \pm 0.18$ for CMIP6 GCMs (the second numbers denote the inter-model standard deviations). The multi-model mean standardized precipitation anomalies are $-0.33 \pm 0.16$ for CMIP5 and $-0.28 \pm 0.14$ for CMIP6 during La Niña states as compared to neutral states (e.g., metric $D1$). Hence, remarkably, all 46 models show positive correlation coefficients between the SST-NINO3.4 and Easter Island P. Moreover, they all simulate precipitation deficits of the order of $-0.3$ standard deviation during La Niña states, whatever their inherent physics and biases.

Regarding model biases, the location of the peak ENSO-related SST anomalies might differ from one model to another. Hence, as mentioned by Cai et al. (2018), using a fixed NINO3.4 region (centered at 0°–145°W) based on observations could affect our results. Based on EOF analyses, we found that the peak of maximal ENSO variability between 5°S and 5°N is located at 156°W ± 25° longitude (the second number is the inter-model standard deviation) for the 25 CMIP5 GCMs, and 152°W ± 15° longitude for the 21 CMIP6 GCMs. For those CMIP5 and CMIP6 GCMs, the averaged locations of peak ENSO variability are thus located in the western half of the NINO3.4 spatial box. Sensitivity studies show that using the location of the peak 5°N-5°S ENSO variability rather than the fixed NINO3.4 spatial box does not change our conclusions.

Two of the models that show a strong correlation between ENSO and Rapa Nui rainfall, the NorESM1-M General Circulation Model (GCM) from CMIP5 and the CESM2 GCM from CMIP6 (Figure 10), are also among the best at simulating ENSO (Bellenger et al., 2014; Planton et al., 2021). They show large-scale correlation patterns similar to those obtained using the CMAP and ERA5 data sets (compare Figures S1a–S1d in Supporting Information S1). To conclude, the analysis of historical simulations from 46-GCMs for the 1850–2014 period corroborates results obtained from the last 4–7 decades. Hence, both the observed and simulated precipitation data sets reveal precipitation deficits on Easter Island ranging from −20% to −30% of the total standard deviation in precipitation during La Niña events.
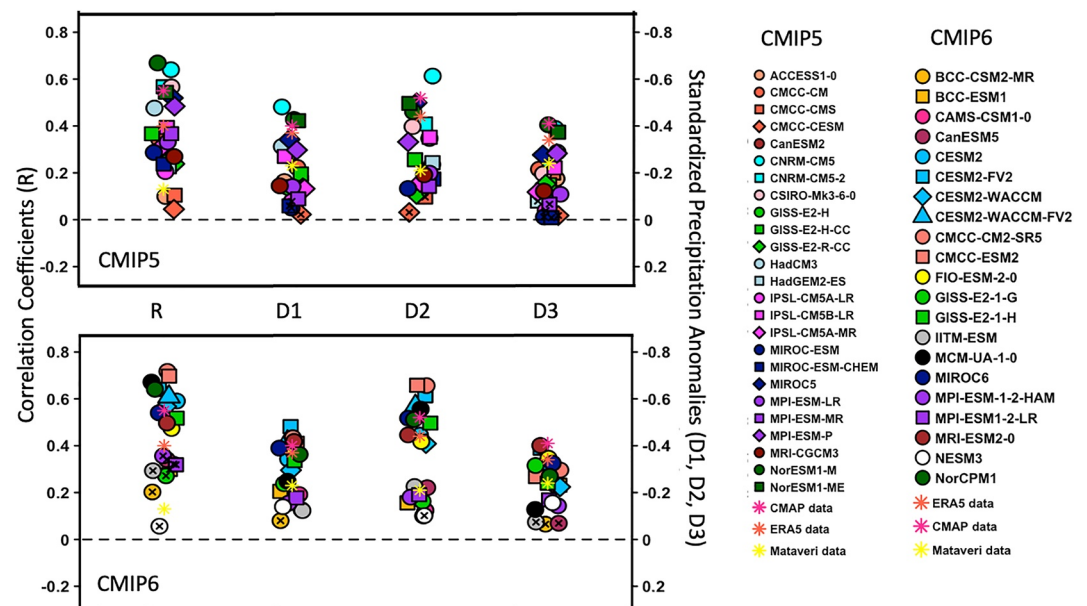
**Figure 10.** Correlation coefficients (*R* column) between the 25-month Hanning filtered and detrended Easter Island precipitation and sea surface temperature (SST)-NINO3.4 values, as derived from 25 Coupled Model Intercomparison Project phase 5 (CMIP5) (top panel) and 21 CMIP6 (bottom panel) General Circulation Models over 1850–2014, scaled on the left vertical axes. Standardized precipitation anomalies between La Niña and neutral situations (*D*1 column), La Niña and El Niño situations (*D*2 column), and La Niña and other situations (*D*3 column), scaled on the right and reversed vertical axes. All significant values at the 90% confidence level, except those marked with an "*x*." Details about the CMIP5 and CMIP6 model names reported on the right are given in Table S1 in Supporting Information S1. Also reported are the *R*, *D*1, *D*2, and *D*3 values derived from the CPC Merged Analysis of Precipitation (red star), ERA5 (orange star), and Mataveri (yellow star) precipitation and SST-NINO3.4 data sets. Mean and standard deviation values of *R*, *D*1, *D*2, and *D*3 are reported in Table 3.

## 4. Pre-Industrial ENSO Variability

The 10-year Hanning filtered time series of our new reconstructed SST-NINO3.4 is shown in Figure 11. The SOI proxy reconstruction of Yan et al. (2011) is overplotted for comparison purposes. Both curves suggest that the tropical Pacific had El Niño-like situations (i.e., warmer-than-average SST in the NINO3.4 box) predominantly during the first third of the last millennium, and La Niña-like situations (i.e., colder-than-average SST in the NINO3.4 box) predominantly during the second and last thirds. Using that 10-year smoothed version, we find that for sliding windows of 30 years (the usual timeframe to define a climate normal), there are about four distinguishable periods with a large fraction of La Niña-like situations (Figure 12). These four periods happened approximately in 1325–1450, 1550–1650, 1725–1750, and 1850–1950, during which some 30-year-long periods experienced more than 80% of La Niña-like events (while the mean over the whole millennium is 34.6%). Another striking feature is the scarcity of La Niña-like events before about 1320. Of the 471 windows of 30-year-length
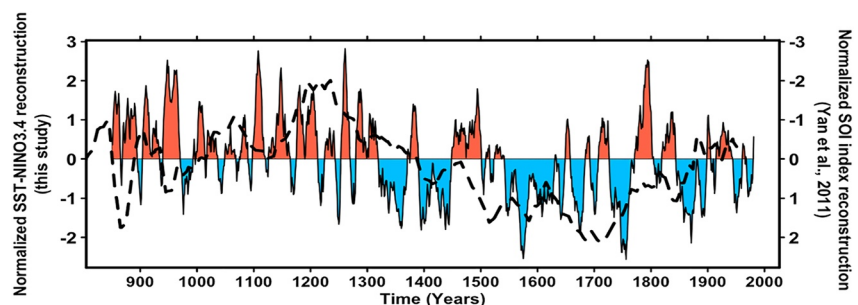


**Figure 11.** Past El Niño Southern Oscillation variability reconstruction. Blue/Red: Time series of the normalized and 10-year Hanning filtered reconstructed sea surface temperature-NINO3.4 index, scaled on the left vertical axis. Heavy dashed line: normalized southern oscillation index proxy reconstruction of Yan et al. (2011), scaled on the right vertical axis.
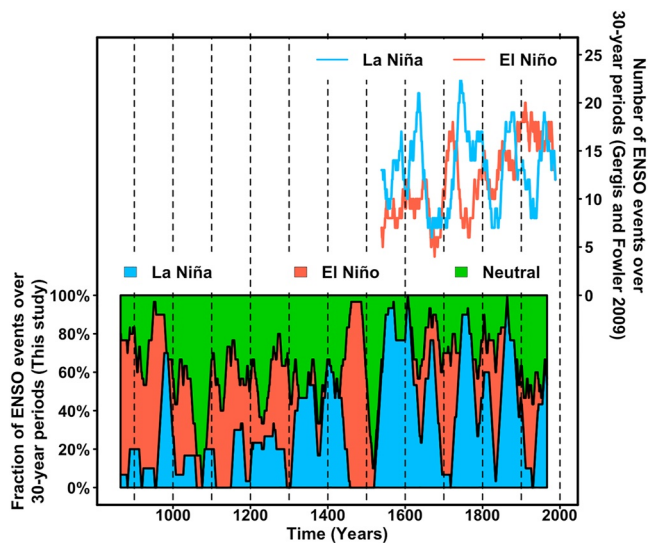
**Figure 12.** (Top panel) Number of La Niña (blue line) and El Niño (red line) events over 30 years sliding windows computed from the ENSO multi-proxy event lists of Gergis and Fowler (2009). (Bottom panel) Relative percentage of La Niña (blue), El Niño (red), and neutral (green) situations over 30 years sliding windows computed from the 10-year Hanning filtered reconstructed SST-NINO3.4 index shown in Figure 11.

before 1320, the average fraction of La Niña-like events is 13.8%, and 21% of these experienced no La Niña-like events at all. By comparison, the 601 sliding windows after 1320 average 49.6% of La Niña-like events, and the percentage without such events is 7.1%. These differences are significant at the 99% confidence levels, suggesting neutral and positive SST-NINO3.4 in the first third of the millennium and fewer during the remaining part.

The background changes in global temperature reconstructed from paleoclimate archives (PAGES 2k Consortium, 2019; IPCC, 2021; Atwood et al., 2021, their Figure 3h) reveal warm anomalies of the order of +0.1°C in the first third of the last millennium and cold anomalies of the order of −0.1°C in the second and last thirds (except for the unprecedented warming after about 1900). This background temperature shift, say around 1300, is consistent with the larger fraction of El Niño-like situations found in the first third of the last millennium, and with the larger fraction of La Niña-like situations found in the second and last thirds. Actually, a portion of the global temperature changes might be attributed to an uneven distribution of El Niño-like/La Niña-like situations, as in recent years (Bulgin et al., 2020). Another way to interpret results of the SST-NINO3.4 reconstruction is that the El Niño-like/La Niña-like situations are modified by low-frequency modes, like the PDO or the IPO.

The analysis of Gergis and Fowler (2009) provides us with an independent estimate of ENSO occurrences from 1525 to 2002. Based on their ENSO multi-proxy event lists (their Table 9), we computed the number of El Niño and La Niña events over 30 years sliding windows (Figure 12), as in McGregor et al. (2010) and Delcroix et al. (2018). By nature, the proxy-based ENSO phase definition of Gergis and Fowler (2010) differs from ours (based on reconstructed SST-NINO3.4 only). Also, about 8% of the 1525–2002 years were classified both as El Niño and La Niña years, depending on the used proxies. However, Figure 12 likewise documents a significant number of La Niña events during the mid-sixteenth, −seventeenth, −eighteenth, and −nineteenth centuries. Furthermore, Gergis and Fowler (their Table 9) detected 13 very strong La Niña events from 1520 to 1660, with a total of 21 events during the period 1622–1649, the longest of which lasted 11 years, from 1622 to 1632. Moreover, the analysis of coral core collected at Palmyra Atoll located in the Central Equatorial Pacific (about 1° to the north of the NINO3.4 box) reveals that the most intense reconstructed ENSO activity over (part of) the last millennium occurred during the mid-seventeenth century (Cobb et al., 2003; Grothe et al., 2019). Interestingly, Wolter and Timlin (2011) demonstrate an almost linear relationship between the duration and the amplitude of the 1871–2005 ENSO phases; hence, the more prolonged the La Niña events, the stronger the related anomalies. Projection of these findings, especially to the fifteenth to seventeenth centuries (see Figure 3), suggests Easter Island should have experienced exceptional and long-lasting precipitation deficits during this period.

## 5. Discussion

A number of studies have already documented close relationships between large-scale climate indices, regional precipitation changes and droughts (e.g., see Mishra & Singh, 2010). We know, especially, that ENSO events did induce precipitation deficits and subsequent droughts in many regions of the planet (e.g., Barlow et al., 2002; Glantz, 1996; Hoerling & Kumar, 2003). Here, we have analyzed the impact of ENSO on Easter Island precipitation changes, with the objective of evaluating the possible related effects on past forest clearing. We analyzed relationships between ENSO and Easter Island precipitation using: (a) in situ, satellite-derived, and reanalysis precipitation products covering the last 4 to 7 decades, (b) 46 historical GCM simulations (25 CMIP5 and 21 CMIP6) covering the last 1.5 centuries, and (c) a new reconstruction of the SST-NINO3.4 ENSO index covering the last millennium.

Results based on in situ, satellite-derived, reanalysis products, and GCM simulations overall document below-normal precipitation during La Niña events and a tendency for above-normal precipitation during El Niño events. We obtained similar conclusions when comparing the Eastern Pacific versus Central Pacific El

Niño events, and Eastern Pacific versus Central Pacific La Niña events. Remarkably, precipitation anomalies are consistently negative for all data types during La Niña events as compared to neutral situations, with a precipitation deficit of the order of −0.2 to −0.4 standardized anomalies (see metric $D1$ in Table 3). To put this estimate in perspective, using a mean precipitation of $0.9 \pm 0.7$ m/year (based on the CMAP, ERA5, and Mataveri values in Section 3.1), this gives a −0.16 to −0.32 m freshwater deficit over the average duration (13.5 months) of the present-day La Niña events, equivalent to the lack of precipitation for 2–5 months (see Figure 6). That deficit is likely related to the westward shift of the mean SPCZ position documented for contemporary La Niña events (Folland et al., 2002), yielding drier conditions near Easter Island.

Results based on our new SST-NINO3.4 reconstruction indicate rare (<7%) occurrences of La Niña-like situations during the first third of the last millennium, and more frequent occurrences (>49%) afterward. Such a shift is consistent with the multidecadal variability in global temperature during the last millennium (PAGES 2k Consortium, 2019; IPCC, 2021), as well as with a strengthening of the Pacific Walker circulation during the LIA relative to the MWP (Atwood et al., 2021; Griffins et al., 2016). The largest occurrences of La Niña-like situations happen especially during four periods, 1325–1450, 1550–1650, 1725–1750, and 1850–1950, when fractions of La Niña-like situations can even exceed 80% in our reconstruction of ENSO. Periods of large La Niña-like occurrences are overall consistent with the independent analysis of the 1525–2002 ENSO multi-proxy annual event lists of Gergis and Fowler (2009; see also Figure 12). Based on present-day values, periods in which fractions of La Niña-like situations exceed 80% would yield a −3.4 to −6.8 m precipitation deficit over 30 years, which is equivalent to the lack of precipitation for 4–7 normal years. Wolter and Timlin (2011) revealed a quasi-linear relationship between duration and amplitude of La Niña events over 1871–2005. We can thus expect such a precipitation deficit to be even underestimated, assuming the relationship still applies when fractions of La Niña-like situations exceed 80%. We conclude that La Niña-like situations after about 1300, especially during the fifteenth to seventeenth centuries, yielded notable and long-lasting precipitation deficits over Easter Island. Whether or not this could also be partly related to a westward shift of the eastern portion of the SPCZ at that time is not clear. Higgins et al. (2020) show that the MWP was characterized by an eastward-shifted SPCZ, while a westward-shifted SPCZ was not discernible in their reconstructed SPCZ index during the LIA.

If Easter Island experienced a greater La Niña-related precipitation deficit during the fifteenth to seventeenth centuries, would this have impacted forest clearing? For the Rano Aroi, the timing of the deficit is remarkably coherent with palm reduction, grass expansion, an increase in charcoal (fires), and Al/Fe concentrations beginning around 1550 (Roman et al., 2021; Rull et al., 2015; see Figure 3). The timing is also consistent with the forest clearing and increased charcoal concentrations reported at the Rano Kao (Seco et al., 2019), as well as changes in the use of cooking fuel in traditional ovens, from the burning of wood to the burning of grass over the whole island (Orliac & Orliac, 2008). It is then reasonable to hypothesize that the La Niña-related protracted precipitation deficit might have played a role in the forest clearing of this island at that moment, on top of other stressors. Notwithstanding, we cannot disregard that the forest clearing was not homogenous in space and time over the island, partly because it was unambiguously modulated by human activities (see Rull, 2020). Moreover, in addition to reduced water supply and human impacts, poor soil fertility, species interactions, contrasted topography, possibly uncontrolled fires, higher wind speed (see below), and combinations of all these factors could have enhanced the severity of droughts and subsequently exacerbated forest loss (Eiserhardt et al., 2011; Fritts, 2021; Lemburg et al., 2016).

Our ENSO SST-NINO3.4 index reconstruction is based on a state-of-the-art statistical approach and uses most of existing proxy records. We should, however, keep in mind that our findings for the last millennium apply to our specific ENSO index reconstruction. A large number of ENSO reconstructions exists in the literature (see Section 2.3, and the review in Emile-Geay et al., 2020). How our findings may differ using other reconstructions clearly remains to be determined. Such an exhaustive comparison is beyond the scope of the present study. Still, we can notice that some former reconstructions (Emile-Geay et al., 2013a, 2013b; M. E. Mann et al., 2009) do not appear to clearly highlight such behavior of ENSO variability, especially in the fifteenth to seventeenth centuries. In contrast, the more recent reconstruction of Loope et al. (2020) seems more in line with our results over the seventeenth to twentieth common analyzed period. Also, it is possible that our reconstruction better extracts low-frequency variations related to IPO variations, notably given the low variability we observed in the fifteenth to seventeenth centuries. Another key source of uncertainty remains related to age model uncertainty of the proxy records (Comboul et al., 2014), which may clearly blur our reconstruction of individual events. We thus argue that changes in the fifteenth to seventeenth centuries might be possibly influenced by IPO variations, which is also

usually associated with ENSO variations. Clearly, additional work comparing multiple available reconstructions is necessary to thoroughly assess the validity of our new reconstruction relative to other attempts, determine their extend of agreement and its sensitivity to age-model uncertainty from proxy records.

Among the various causes of forest demise, another interesting perspective, still related to ENSO changes, would be to quantify the effects of the surface wind field and related evapotranspiration changes. The preliminary analysis of Delcroix et al. (2018) based on the 1979–2015 ERA_I monthly records (Dee et al., 2011) indicates stronger-than-normal (weaker-than-normal) zonal surface winds during La Niña (El Niño) events of the order of ±15% of the mean. (Recall surface winds are predominantly easterlies over Easter Island (see Steiger et al., 2022), hence the reason why these authors only looked at zonal components). The stronger-than-normal zonal surface wind during La Niña events might subsequently enhance evapotranspiration, reinforcing the precipitation deficit for the soil moisture and drought condition, detrimental to the local plants. The monthly wind data used by Delcroix et al. (2018) was, however, too much under-sampled to accurately compute wind speed (during 1 month, for instance, the monthly mean zonal component is zero with the wind blowing 50% eastward and 50% westward at 10 m/s, whereas the mean speed is 10 m/s). It would thus be interesting to precisely quantify the ENSO-related evapotranspiration changes from high temporal resolution wind products and a large number of meteorological variables (see Allen et al., 1998), such as temperature, solar radiation, and relative humidity, not all of which recorded at meteorological stations, together with information on land cover patterns. An alternative to tentatively clarify the issue would be to test the sensibility of evapotranspiration models (e.g., Guo et al., 2017) as well as Easter Island vegetation models to ENSO-related fluctuations. To our knowledge, the latter is, however, poorly settled at the moment.

Since the pioneering efforts of Heyerdahl and Ferdon (1961) and Flenley and King (1984) through more recently published analyses (See Rull, 2021, for a review), the temporal resolution of the pollen records performed on sedimentary cores used to infer landscape changes has improved significantly. As documented by Margalef et al. (2013) and most recently by Roman et al. (2021), high-time resolution of trace and rare earth elements proved quite promising for better inferring the abruptness of any changes. However, the timing of the landscape changes over Easter Island remains relatively imprecise, given the inherent large error bars on age-depth models. There is, therefore, a definite need to improve such models to investigate interannual to decadal changes more thoroughly.

Our study suggests protracted La Niña-related precipitation deficits were detrimental to the forest coverage, especially during the fifteenth to seventeenth century. From a statistical standpoint, these long-lasting deficits faced by the Rapa Nui people were extreme (unusual) events, then of natural origin, in contrast with the extreme events we experience in today's climate crisis (IPCC, 2021). Regardless of their causes, extreme events are most of the time harmful to the environment. However, it would not be relevant to simply infer that such extreme events further had a major impact on Easter Island cultural evolution (for instance, on the shift from the moai to the birdman cult) given complexities of climate-society interactions (Degroot et al., 2021; Zhang et al., 2007). It is then obvious that only multi-disciplinary and cross-cutting research may improve our understanding of Easter Island cultural evolution (cf. Rull et al., 2018).

## Data Availability Statement

The precipitation data we used are from (a) CPC Merged Analysis of Precipitation (CMAP): https://psl.noaa.gov/data/gridded/data.cmap.html (Xie & Arkin, 1997), (b) ERA5 (Hersbach et al., 2019, 2020), and (c) Mataveri: https://climatologia.meteochile.gob.cl/application/requerimiento/producto/RE1006/270001 (Only available in Spanish). The 1870–2021 sea surface temperature data are from HadISST: https://www.metoffice.gov.uk/hadobs/hadisst/ (Rayner et al., 2003). The 1525–2002 ENSO event list is available from Gergis and Fowler (2009; their Table 9). The PAGES 2k proxy data set (PAGES 2k Consortium, 2017) is available from the NOAA Paleo data search: https://www.ncei.noaa.gov/pub/data/paleo/pages2k/pages2k-temperature-v2-2017/, version 2.0.0. The Coupled Model Intercomparison Project phase 5 (CMIP5) (Taylor et al., 2012) and CMIP6 (Eyring et al., 2016) models used in this study are listed in Table S1 in Supporting Information S1; the model outputs are available from the Institut Pierre Simon Laplace (IPSL) CMIP nodes through the Earth System Grid Federation (ESGF) data portal: https://esgf-node.ipsl.upmc.fr/projects/esgf-ipsl/. The 850–1981 reconstructed SST-NINO3.4 time series generated and analyzed in this study is deposited in a Zenodo repository (Michel, Swingedouw, & Delcroix, 2022). Codes and analyses were integrally made using the *R* (R Core Team, 2019) and Bash Unix (https://www.gnu.org/software/bash/) languages.

# References

Allen, G., Pereira, L., Raes, D., & Smith, M. (1998). Crop evapotranspiration – Guidelines for computing crop water requirements. In *Food and Agriculture Organization (FAO) irrigation and drainage paper N° 56* (p. 15). FAO.

Ashok, K., Behera, S. K., Rao, S. A., Weng, H., & Yamagata, T. (2007). El Niño Modoki and its possible teleconnection. *Journal of Geophysical Research*, *112*(C11), C11007. https://doi.org/10.1029/2006JC003798

Atwood, A. R., Battisti, D. S., Wu, E., Frierson, D. M. W., & Sachs, J. P. (2021). Data-model comparisons of tropical hydroclimate changes over the Common Era. *Paleoceanography and Paleoclimatology*, *36*(7), e2020PA003934. https://doi.org/10.1029/2020PA003934

Bahn, P., & Flenley, J. (1992). Easter Island, Earth Island. *The Enigmas of Rapa Nui* (p. 240). Thames and Hudson Editor.

Bahn, P., & Flenley, J. (2019). Easter Island, Earth Island. *The Enigmas of Rapa Nui* (4th ed.). Publisher Rowman & Littelefield.

Barlow, M., Cullen, H., & Bradfield, L. (2002). Drought in central and southwest Asia: La Niña, the warm pool, and Indian Ocean precipitation. *Journal of Climate*, *15*(7), 697–700. https://doi.org/10.1175/1520-0442(2002)015<0697:dicasa>2.0.co;2

Bellenger, H., Guilyardi, E., Leloup, J., Lengaigne, M., & Vialard, J. (2014). ENSO representation in climate models, from CMIP3 to CMIP5. *Climate Dynamics*, *42*(7–8), 1999–2018. https://doi.org/10.1007/s00382-013-1783-z

Bentsen, M., Bethke, I., Debernard, J. B., Iversen, T., Kirkevåg, A., Seland, Ø., et al. (2013). The Norwegian Earth System Model, NorESM1-M – Part 1: Description and basic evaluation of the physical climate. *Geoscientific Model Development*, *6*(3), 687–720. https://doi.org/10.5194/gmd-6-687-2013

Blaauw, M., & Christen, J. A. (2011). Flexible paleoclimate age-depth models using an autoregressive gamma process. *Bayesian Analysis*, *6*(3), 457–474. https://doi.org/10.1214/11-BA618

Boersema, J. (2015). The survival of Easter Island. *Dwindling resources and cultural resilience* (p. 308). Cambridge University Press.

Bretherton, C. S., Widmann, M., Dymnikov, V. P., Wallace, J. M., & Bladé, I. (1999). The effective number of spatial degrees of freedom on time-varying field. *Journal of Climate*, *12*(7), 1990–2009. https://doi.org/10.1175/1520-0442(1999)012<1990:TENOSD>2.0.CO;2

Bulgin, C. E., Merchant, C. J., & Ferreira, D. (2020). Tendencies, variability and persistence of sea surface temperature anomalies. *Nature Scientific Reports*, *10*(1), 7986. https://doi.org/10.1038/s41598-020-64785-9

Cai, W., Wang, G., Dewitte, B., Wu, L., Santoso, A., Takahashi, K., et al. (2018). Increased variability of eastern Pacific El Niño under greenhouse warming. *Nature*, *564*(7735), 201–206. https://doi.org/10.1038/s41586-018-0776-9

Canellas-Bolta, N., Rull, V., Saez, A., Margalef, O., Bao, R., Pla-Rabes, S., et al. (2013). Vegetation changes and human settlement of Easter Island during the last millennia: A multiproxy study of the Lake Raraku sediments. *Quaternary Science Reviews*, *72*, 36–48. https://doi.org/10.1016/j.quascirev.2013.04.004

Cauwe, N. (2018). *Iles de Pâques. Le Grand Tabou. Dix années de fouilles reconstruisent son histoire* (p. 144). Editions Versant Sud.

Cobb, K. M., Charles, C. D., Cheng, H., & Edwards, L. (2003). El Niño/Southern Oscillation and tropical Pacific climate during the last millennium. *Nature*, *424*(6946), 271–276. https://doi.org/10.1038/nature01779

Comboul, M., Emile-Geay, J., Evans, M. N., Mirnateghi, N., Cobb, K. M., & Thompson, D. M. (2014). A probabilistic model of chronological errors in layer-counted climate proxies: Applications to annually banded coral archives. *Climate of the Past*, *10*(2), 825–841. https://doi.org/10.5194/cp-10-825-2014

Danabasoglu, G., Lamarque, J., Bacmeister, J., Bailey, D. A., DuVivier, A. K., Edwards, J., et al. (2020). The Community Earth System model Version 2 (CESM2). *Journal of Advances in Modeling Earth Systems*, *12*, 12–2. https://doi.org/10.1029/2019MS001916

Dätwyler, C., Abram, N. J., Grosjean, M., Wahl, E. R., & Neukon, R. (2020). El Niño-Southern Oscillation variability, teleconnection changes and responses to large volcanic eruptions since AD 1000. *International Journal of Climatology*, *39–5*(5), 2711–2724. https://doi.org/10.1002/joc.5983

De Lesseps (1861). Voyage de La Pérouse, rédigé d'après ses manuscrits originaux; suivi d'un appendice renfermant tout ce que l'on a découvert depuis le naufrage jusqu'à nos jours, et enrichi de notes. Paris, Arthus Bertrand.

Dee, D. P., Uppala, S. M., Simmons, A. J., Berrisford, P., Poli, P., Kobayashi, S., et al. (2011). The ERA-interim reanalysis: Configuration and performance of the data assimilation system. *Quarterly Journal of the Royal Meteorological Society*, *137*(656), 53–597. https://doi.org/10.1002/qj.828

Degroot, D., Anchukaitis, K., Bauch, M., Burnham, J., Carnegy, F., Cui, J., et al. (2021). Towards a rigorous understanding of societal responses to climate change. *Nature*, *591*(7851), 25–550. https://doi.org/10.1038/s41586-021-03190-2

Delcroix, T. (1998). Observed surface oceanic and atmospheric variability in the Tropical Pacific at seasonal and ENSO time scales: A tentative overview. *Journal of Geophysical Research*, *103*(C9), 18611–18633. https://doi.org/10.1029/98JC00814

Delcroix, T., Abarca-del-Rio, R., Corrège, T., & Malaizé, B. (2018). Le phénomène La Niña et la 'catastrophe écologique' de l'île de Pâques. *La Météorologie*, *102*, 42–48. https://doi.org/10.4267/2042/68212

Diamond, J. (2005). *Collapse: How societies chose to fail or succeed*. Penguin books.

DiNapoli, R. J., Crema, E. R., Lipo, C. P., Rieth, T. M., & Hunt, T. L. (2021). Approximate Bayesian computation of radiocarbon and paleoenvironmental record shows population resilience on Rapa Nui (Easter Island). *Nature Communications*, *12*(1), 3939. https://doi.org/10.1038/s41467-021-24252-z

Dransfield, J., Flenley, J., King, S., & Rapu, S. (1984). A recently extinct palm from Easter Island. *Nature*, *312*(5996), 750–752. https://doi.org/10.1038/312750a0

Eiserhardt, W., Svenning, J.-S., Kissling, W., & Balslev, H. (2011). Geographical ecology of the palms (Arecaceae): Determinants of diversity and distributions across spatial scales. *Annals of Botany*, *108*(8), 1391–1416. https://doi.org/10.1093/aob/mcr146

Emile-Geay, J., Cobb, K. M., Cole, J. E., Elliot, M., & Zhu, F. (2020). Past ENSO variability. *Geophysical monograph series*, (p. 528). American Geophysical Union Publications. https://doi.org/10.1002/9781119548164.ch5

Emile-Geay, J., Cobb, K. M., Mann, M. E., & Wittenberg, A. T. (2013a). Estimating tropical Pacific SST variability over the past millennium. Part 1: Methodology and validation. *Journal of Climate*, *26*(7), 2302–2328. https://doi.org/10.1175/JCLI-D-11-00510.1

Emile-Geay, J., Cobb, K. M., Mann, M. E., & Wittenberg, A. T. (2013b). Estimating tropical Pacific SST variability over the past millennium. Part 2: Reconstructions and uncertainties. *Journal of Climate*, *26*(7), 2329–2352. https://doi.org/10.1175/JCLI-D-11-00511.1

Eyring, V., Bony, S., Meehl, G. A., Senior, C. A., Stevens, B., Stouffer, R. J., & Taylor, K. E. (2016). Overview of the coupled model Intercomparison project phase 6 (CMIP6) experimental design and organization. *Geoscientific Model Development*, *9*(5), 1937–1958. https://doi.org/10.5194/gmd-9-1937-2016

Flenley, J. R., & King, S. M. (1984). Late Quaternary pollen records from Easter Island. *Nature*, *307*(5946), 47–50. https://doi.org/10.1038/307047a0

Flenley, J. R., Teller, J. T., Sarah, A., King, M., Jackson, J., Chew, C., et al. (1991). The Late Quaternary vegetational and climatic history of Easter Island. *Journal of Quaternary Science*, *6–2*(2), 85–115. https://doi.org/10.1002/jqs.3390060202

Folland, C. K., Renwick, J. A., Salinger, M. J., & Mullan, A. B. (2002). Relative influence of the interdecadal Pacific oscillation and ENSO on the South Pacific Convergence Zone. *Geophysical Research Letters*, *29*(13), 1643. https://doi.org/10.1029/2001GL014201

Fritts, R. (2021). Settlement of Rapa Nui may have been doomed by a dearth of dust. *Eos*, *102*. https://doi.org/10.1029/2021EO210640

Genz, J., & Hunt, T. (2003). El Niño/Southern Oscillation and Rapa Nui prehistory. *Rapa Nui Journal*, *17*, 7–14.

Gergis, J., & Fowler, A. (2009). A history of ENSO events since AD 1525: Implications for future climate change. *Climate Change*, *92*(3–4), 343–387. https://doi.org/10.1007/s10584-008-9476-z

Glantz, M. (1996). *Currents of change. El Niño's impact on climate and society* (p. 194). Cambridge University Press.

Griffins, M., Kimbrough, A., Gagan, M., Drysdale, R. N., Cole, J. E., Johnson, K. R., et al. (2016). Western Pacific hydroclimate linked to global climate variability over the past two millennia. *Nature Communications*, *7*(1), 11719. https://doi.org/10.1038/ncomms11719

Grothe, P. R., Cobb, K. M., Liguori, G., Di Lorenzo, E., Capotondi, A., Lu, Y., et al. (2019). Enhanced El Niño–Southern oscillation variability in recent decades. *Geophysical Research Letters*, *46*(7), e2019GL083906. https://doi.org/10.1029/2019GL083906

Guo, D., Westra, S., & Maier, H. R. (2017). Sensitivity of potential evapotranspiration to changes in climate variables for different Australian climatic zones. *Hydrology and Earth System Sciences*, *21*(4), 2107–2126. https://doi.org/10.5194/hess-21-2107-2017

Hanley, D., Bourassa, M., O'Brien, J. J., Smith, S., & Spade, E. (2003). A quantitative evaluation of ENSO indices. *Journal of Climate*, *16*(8), 249–1258. https://doi.org/10.1175/1520-0442(2003)16

Henley, B. J., Gergis, J., Karoly, D. J., Power, S., Kennedy, J., & Folland, C. F. (2015). A tripole index for the interdecadal Pacific oscillation. *Climate Dynamics*, *45*(11–12), 3077–3090. https://doi.org/10.1007/s00382-015-2525-1

Hersbach, H., Bell, B., Berrisford, P., Biavati, G., Horányi, A., Muñoz Sabater, J., et al. (2019). ERA5 monthly averaged data on single levels from 1959 to present. Copernicus Climate Change Service (C3S) Climate Data Store (CDS). [Dataset]. https://doi.org/10.24381/cds.f17050d7

Hersbach, H., Bell, B., Berrisford, P., Hirahara, S., Horanyi, A., Munoz-Sabater, J., et al. (2020). The ERA5 global reanalysis. *Quaternary Journal of the Royal Meteorological Society*, *146–730*(730), 1999–2049. https://doi.org/10.1002/qj.3803

Heyerdahl, T., & Ferdon, E. (1961). Archaeology of Easter Island. *Reports of the Norwegian archaeological expedition to Easter Island and the East Pacific* (Vol. 1, p. 559). Rand McNally Company/Monographs of the School of American Research and the Museum of New Mexico.

Higgins, P. A., Palmer, J. G., Turney, C. S. M., Andersen, M. S., & Cook, E. R. (2020). One thousand three hundred years of variability in the position of the South Pacific Convergence Zone. *Geophysical Research Letters*, *47*(17), e2020GL088238. https://doi.org/10.1029/2020GL088238

Hoerling, M., & Kumar, A. (2003). The perfect ocean for drought. *Science*, *299*(5607), 691–694. https://doi.org/10.1126/science.1079053

Hogg, A., Heaton, T., Hua, Q., Palmer, J., Turney, C., Southon, J., et al. (2020). SHCal20 southern hemisphere calibration, 0–55,000 Years cal BP. *Radiocarbon*, *62*(4), 759–778. https://doi.org/10.1017/RDC.2020.59

Hsu, C. P. F., & Wallace, J. M. (1976). The global distribution of the annual and semiannual cycles in precipitation. *Monthly Weather Review*, *104*(9), 1093–1101. https://doi.org/10.1175/1520-0493(1976)104%3C1093:TGDOTA%3E2.0.CO;2

Hu, Z. Z., Kumar, A., Xue, Y., & Jha, B. (2014). Why were some La Niña followed by another La Niña? *Climate Dynamics*, *42*(3–4), 1029–1042. https://doi.org/10.1007/s00382-013-1917-3

Hunt, T. L. (2007). Rethinking Easter Island's ecological catastrophe. *Journal of Archaeological Science*, *34*(3), 485–502. https://doi.org/10.1016/j.jas.2006.10.003

Hunt, T. L., & Lipo, C. P. (2006). Late colonization of easter island. *Science*, *311*(5767), 1603–1606. https://doi.org/10.1126/science.1121879

Hunt, T. L., & Lipo, C. P. (2011). *The statues that walked: Unraveling the mystery of Easter Island* (p. 258). Free Press Edition.

IPCC. (2021). Summary for policymakers. In *Climate change 2021: The physical science basis. Contribution of working group I to the sixth assessment report of the intergovernmental panel on climate change*. Cambridge University Press.

Junk, C., & Claussen, M. (2011). Simulated climate variability in the region of Rapa Nui during the last millennium. *Climate of the Past*, *7*(2), 579–586. https://doi.org/10.5194/cp-7-579-2011

Kao, H. Y., & Yu, J. Y. (2009). Contrasting eastern-Pacific and central-Pacific types of ENSO. *Journal of Climate*, *22*(3), 615–632. https://doi.org/10.1175/2008JCLI2309.1

Kug, J.-S., Jin, F.-F., & An, S.-I. (2009). Two types of El Niño events: Cold tongue El Niño and warm pool El Niño. *Journal of Climate*, *22*(6), 1499–1515. https://doi.org/10.1175/2008JCLI2624.1

Lemburg, A., Claussen, M., & Ament, F. (2016). Deforestation decreases resistance of simulated Easter Island climate to drought. Climate of the Past Discussions. [preprint]. Retrieved from 10.5194/cp-2016-68

Li, J., Xie, S. P., Cook, E. R., Morales, M. S., Christie, D. A., Johnson, N. C., et al. (2013). El Niño modulations over the past seven centuries. *Nature Climate Change*, *3*(9), 822–826. https://doi.org/10.1038/NCLIMATE1936

Lima, M., Gayo, E. M., Latorre, C., Santoro, C. M., Estay, S. A., Cañellas-Boltà, N., et al. (2020). Ecology of the collapse of Rapa Nui society. *Proceedings of the Royal Society B*, *287*(1929), 20200662. https://doi.org/10.1098/rspb.2020.0662

Linscheid, N., Estupinan-Suarez, L. M., Brenning, A., Carvalhais, N., Cremer, F., Gans, F., et al. (2020). Towards a global understanding of vegetation–climate dynamics at multiple timescales. *Biogeosciences*, *17*(4), 945–962. https://doi.org/10.5194/bg-17-945-2020

Loope, G., Thompson, D., Cole, J., & Overpeck, J. (2020). Is there a low-frequency bias in multiproxy reconstructions of tropical Pacific SST variability? *Quaternary Science Reviews*, *246*, 106530. https://doi.org/10.1016/j.quascirev.2020.106530

MacIntyre, F. (2001). ENSO, climate variability, and the Rapa Nui, part II. Oceanography and Rapa Nui. *Rapa Nui Journal*, *15*(2), 83–94.

Mann, D., Edwards, J., Chase, J., Beck, W., Reanier, R., Mass, M., et al. (2008). Drought, vegetation change, and human history on Rapa Nui (Isla de Pascua, Easter Island). *Quaternary Research*, *69*(1), 16–28. https://doi.org/10.1016/j.yqres.2007.10.009

Mann, M. E., Zhang, Z., Rutherford, S., Bradley, R. S., Hughes, M. K., Shindell, D., et al. (2009). Global signature and dynamical origins of the Little Ice Age and medieval climate anomaly. *Science*, *326*(22 November 2009), 1256–1260. https://doi.org/10.1126/science.1177303

Margalef, O., Canellas-Bolta, N., Pla-Rabes, S., Giralt, S., Pueyo, J. J., Joosten, H., et al. (2013). A 70,000 year multiproxy record of climatic and environmental change from Rano Aroi peatland (Easter Island). *Global and Planetary Change*, *108*, 72–84. https://doi.org/10.1016/j.gloplacha.2013.05.016

McCall, G. (1993). Little Ice Age: Some speculations for Rapa Nui. *Rapa Nui Journal*, *7–4*, 65–70.

McGregor, S., Timmermann, A., England, M. H., Timm, O. E., & Wittenberg, A. T. (2013). Inferred changes in El Niño–Southern Oscillation variance over the past six centuries. *Climate of the Past*, *9*(5), 2269–2284. https://doi.org/10.5194/cp-9-2269-2013

McGregor, S., Timmermann, A., & Timm, O. (2010). A unified proxy for ENSO and PDO variability since 1650. *Climate of the Past*, *6*, 1–17. https://doi.org/10.5194/cp-6-1-2010

Michel, S., Swingedouw, D., Chavent, M., Ortega, P., Mignot, J., & Khodri, M. (2020). Reconstructing climatic modes of variability using CimIndRec version 1.0. *Geoscientific Model Development*, *13*(2), 841–858. https://doi.org/10.5194/gmd-13-841-2020

Michel, S. L. L., Swingedouw, D., & Delcroix, T. (2022). Reconstructed SST-NINO3.4 anomalies for the years 850 to 1981 (v1.0). [Dataset]. Zenodo. Retrieved from 10.5281/zenodo.6926595

Michel, S. L. L., Swingedouw, D., Ortega, P., Gastineau, G., Mignot, J., McCarthy, D., & Khodri, M. (2022). Early warning signal for a tipping point suggested by a millennial Atlantic Multidecadal Variability reconstruction. *Nature Communications*, *13*(1), 5179. https://doi.org/10.1038/s41467-022-32704-3

Mishra, A., & Singh, V. (2010). A review of drought concepts. *Journal of Hydrology*, *391*(1–2), 202–216. https://doi.org/10.1016/j.jhydrol.2010.07.012

Mucciarone, D. A., & Dunbar, R. B. (2003). Stable isotope record of El Niño-Southern Oscillation events from easter island. In J. Loret & J. T. Tanacredi (Eds.), *Easter Island*. Springer. https://doi.org/10.1007/978-1-4615-0183-1_8

Nash, J. E., & Sutcliffe, J. V. (1970). River flow forecasting through conceptual models. Part I: A discussion of principles. *Journal of Climatology*, *10*(3), 282–290. https://doi.org/10.1016/0022-1694(70)90255-6

Newman, M., Alexander, M. A. A., Ault, T. R., Cobb, K. M., Deser, C., Di Lorenzo, E., et al. (2016). The Pacific decadal oscillation, revisited. *Journal of Climate*, *29*(12), 4399–4427. https://doi.org/10.1175/JCLI-D-15-0508.1

Nicet, J.-B., & Delcroix, T. (2000). ENSO-related precipitation changes in New Caledonia, South Western Tropical Pacific. 1969-1998. *Monthly Weather Review*, *128*, 3001–3006. https://doi.org/10.1175/1520-0493(2000)128%3C3001:ERPCIN%3E2.0.CO;2

Orliac, C. (2000). The woody vegetation of Easter Island between the early 14th to the mid-17th centuries AD. In C. M. Stevenson & W. S. Ayres (Eds.), *Easter Island archaeology: Research on Early Rapa Nui culture* (pp. 199–207). Easter Island Foundation.

Orliac, C., & Orliac, M. (1998). The disappearance of Easter Islands's forest: Over-exploitation or climatic catastrophe. In C. M. Stevenson, G. Lee, & F. J. Morin (Eds.), *Easter Island in Pacific context. Proceedings of the 4th international conference on easter island and east Polynesia, Easter Island Foundation* (Vol. *4*, pp. 129–144).

Orliac, C., & Orliac, M. (2008). Extinct flora of Easter Island. In A. Di Piazza, E. Pearthree, & C. Sand (Eds.), *At the heart of ancient societies, French contributions to pacific archaeology*, *Les Cahiers de l'Archéologie en Nouvelle-Calédonie* (Vol. *18*, pp. 197–208).

Ortlieb, L. (2000). *The documented historical record of El Niño events in Peru: An update of the Quinn record (XVI to XIX centuries)* (pp. 207–295). Cambridge University Press.

PAGES 2k Consortium. (2017). A global multiproxy database for temperature reconstructions of the Common Era. *Scientific Data*, *4*(1), 170088. https://doi.org/10.1038/sdata.2017.88

PAGES 2k Consortium. (2019). Consistent multidecadal variability in global temperature reconstructions and simulations over the Common Era. *Nature Geoscience*, *12*(8), 643–649. https://doi.org/10.1038/s41561-019-0400-0

Philander, S. G. (1989). *El Niño, La Niña, and the southern oscillation* (Vol. 46, p. 293). Academic press inc. International Geophysics Series.

Picaut, J., Ioualalen, M., Menkes, C., Delcroix, T., & McPhaden, M. (1996). Mechanism of the zonal displacements of the Pacific Warm Pool, implications for ENSO. *Science*, *274*(5292), 1486–1489. https://doi.org/10.1126/science.274.5292.1486

Planton, Y., Guilyardi, E., Wittenberg, A., Lee, L., Gleckler, P., Bayr, T., et al. (2021). Evaluating climate models with the CLIVAR 2020 ENSO metrics package. *Bulletin of the American Metorological Society*, *102*(2), E193–E217. https://doi.org/10.1175/bams-d-19-0337.1

Power, S., Lengaigne, M., Capotondi, A., Khodri, M., Vialard, J., Jebri, B., et al. (2021). Decadal climate variability in the tropical Pacific: Characteristics, causes, predictability and prospects. *Science*, *374*, 374–6563. https://doi.org/10.1126/science.aay9165

Preble, M., & Dowe, J. L. (2008). The late Quaternary decline and extinction of palms on oceanic Pacific islands. *Quaternary Science Reviews*, *27*(27–28), 2546–2567. https://doi.org/10.1016/j.quascirev.2008.09.015

Rayner, N. A., Parker, D. E., Horton, E. B., Folland, C. K., Alexander, L. V., Rowell, D. P., et al. (2003). Global analyses of sea surface temperature, sea ice, and night marine air temperature since the late nineteenth century. *Journal of Geophysical Research*, *108*(D14), 4407. https://doi.org/10.1029/2002JD002670

R Core Team. (2019). R: A language and environment for statistical computing. R Foundation for Statistical Computing. [Software]. Retrieved from http://www.R-project.org/

Rodgers, K. B., Friederichs, P., & Latif, M. (2004). Tropical Pacific decadal variability and its relation to decadal modulations of ENSO. *Journal of Climate*, *17*(19), 3761–3774. https://doi.org/10.1175/1520-0442(2004)017<3761:TPDVAI>2.0.CO;2

Roman, M., McWethy, D. B., Kehrwald, N. M., Erhenhi, E. O., Myrbo, A. E., Ramirez-Aliaga, J. M., et al. (2021). A multi-decadal geochemical record from Rano Aroi (Easter Island/Rapa Nui): Implications for the environment, climate and humans during the last two millennia. *Quaternary Science Reviews*, *268*, 268–107115. https://doi.org/10.1016/j.quascirev.2021.107115

Rull, V. (2020). The deforestation of Easter Island. *Biological Reviews*, *95*(1), 124–141. https://doi.org/10.1111/brv.12556

Rull, V. (2021). Contributions of paleoecology to easter Island's prehistory: A thorough review. *Quaternary Science Reviews*, *252*, 106751. https://doi.org/10.1016/j.quascirev.2020.106751

Rull, V., Cañellas-Boltà, N., Margalef, O., Sàez, A., Pla-Rabes, S., & Giralt, S. (2015). Late Holocene vegetation dynamics and deforestation in Rano Aroi: Implications for Easter Island's ecological and cultural history. *Quaternary Science Reviews*, *126*, 219–226. https://doi.org/10.1016/j.quascirev.2015.09.008

Rull, V., Montoya, E., Seco, I., Cañellas-Boltà, N., Giralt, S., Margalef, O., et al. (2018). CLAFS, a holistic climatic-ecological-anthropogenic hypothesis on Easter Island's deforestation and cultural change: Proposals and testing prospects. *Frontiers in Ecology and Evolution*, *6*, 32. https://doi.org/10.3389/fevo.2018.00032

Salinger, M. J., Renwick, J. A., & Mullan, A. B. (2001). Interdecadal Pacific oscillation and south Pacific climate. *International Journal of Climatology*, *21*(14), 1705–1721. https://doi.org/10.1002/joc.691

Seco, I., Rull, V., Montoya, E., Canellas-Bolta, N., Giralt, S., Margalef, O., et al. (2019). A continuous palynological record of forest clearing at Rano Kao (Easter Island, SE Pacific) during the last millennium: Preliminary report. *Quaternary*, *2*, 22. https://doi.org/10.3390/quat2020022

Singh, A., Delcroix, T., & Cravatte, S. (2011). Contrasting the flavours of El Niño Southern Oscillation using sea surface salinity observations. *Journal of Geophysical Research*, *116*(C6), C06016. https://doi.org/10.1029/2010JC006862

Steiger, N. J., D'Andrea, W. J., Smerdon, J. E., & Bradley, R. S. (2022). Large infrequent rain events dominate the hydroclimate of Rapa Nui (Easter Island). *Climate Dynamics*, *59*(1–2), 595–608. https://doi.org/10.1007/s00382-022-06143-1

Stevenson, C. M., Puleston, C. O., Vitousek, P. M., Chadwick, O. A., Haoa, S., & Ladefoged, T. N. (2015). Variation in Rapa Nui (Easter Island) land use indicates production and population peaks prior to European contact. *Proceedings of the National Academy of Sciences of the USA*, *112*(4), 1025–1030. https://doi.org/10.1073/pnas.1420712112

Sun, Q., Miao, C., Duan, Q., Ashouri, H., Sorooshian, S., & Hsu, K. L. (2018). A review of global precipitation data sets: Data sources, estimation, and intercomparisons. *Reviews of Geophysics*, *56*(1), 79–107. https://doi.org/10.1002/2017RG000574

Sun, T., & Okumura, Y. M. (2020). Impact of ENSO-like tropical Pacific decadal variability on the relative frequency of El Niño and La Niña Events. *Geophysical Research Letters*, *47*, 47–53. https://doi.org/10.1029/2019GL085832

Taylor, K. E., Stouffer, R. J., & Meehl, G. A. (2012). An overview of CMIP5 and the experiment design. *Bulletin of the American Meteorological Society*, *93*(4), 485–497. https://doi.org/10.1175/BAMS-D-11-00094.1

Tchilibou, M., Delcroix, T., Alory, G., Arnault, S., & Reverdin, G. (2015). Variations of the Tropical Atlantic and Pacific SSS minimum zones and their relations to the ITCZ and SPCZ rain bands (1979-2009). *Journal of Geophysical Research*, *120*(7), 5090–5100. https://doi.org/10.1002/2015JC010836

Tourre, Y., Rajagopalan, B., Kushnir, Y., Barlow, M., & White, W. (2001). Patterns of coherent decadal and interdecadal climate signals in the Pacific basin during the 20th century. *Geophysical Research Letters*, *28*(10), 2069–2072. https://doi.org/10.1029/2000GL012780

Trenberth, K. E., & Caron, J. M. (2000). The southern oscillation revisited: Sea level pressure, surface temperatures and precipitation. *Journal of Climate*, *13*(24), 4358–4365. https://doi.org/10.1175/1520-0442(2000)013%3C4358:TSORSL%3E2.0.CO;2

Trenberth, K. E., & Stepaniak, D. P. (2001). Indices of El Niño evolution. *Journal of Climate*, *14*(8), 1697–1701. https://doi.org/10.1175/1520-0442(2001)014%3C1697:LIOENO%3E2.0.CO;2

van der Werf, G. R., Randerson, J. T., Giglio, L., Gobron, N., & Dolman, A. J. (2008). Climate controls on the variability of fires in the tropics and subtropics. *Global Biogeochemical Cycles*, *22*(3). https://doi.org/10.1029/2007GB003122

Wolter, K., & Timlin, M. (2011). El Niño/Southern Oscillation behavior since 1871 as diagnosed in an extended multivariate ENSO index (MEI. ext). *International Journal of Climate*, *31*(7), 1074–1087. https://doi.org/10.1002/joc.2336

Xie, P., & Arkin, P. (1997). Global precipitation: A 17-year monthly analysis based on gauge observations, satellite estimates, and numerical model outputs. *Bulletin of the American Meteorological Society*, *78*, 2539–2558. https://doi.org/10.1175/1520-0477(1997)078%3C2539:GPAYMA%3E2.0.CO;2

Yan, H., Sun, L., Wang, Y., Huang, W., Qiu, S., & Yang, C. (2011). A record of the southern oscillation index for the past 2,000 years from precipitation proxies. *Nature Geoscience*, *4*(9), 611–614. https://doi.org/10.1038/ngeo1231

Zhang, D. D., Brecke, P., Lee, H. F., He, Y. Q., & Zhang, J. (2007). Global climate change, war, and population decline in recent human history. *Proceedings of the National Academy of Sciences of the USA*, *104*(49), 19214–19219. https://doi.org/10.1073/pnas.0703073104